

MARÍA JOSÉ BALART, JAYESH B. PATEL, FENG GAO, and ZHONGYUN FAN

This study reports the current status of grain refinement of copper accompanied in particular by a critical appraisal of grain refinement of phosphorus-deoxidized, high residual P (DHP) copper microalloyed with 150 ppm Ag. Some deviations exist in terms of the growth restriction factor ( $Q$ ) framework, on the basis of empirical evidence reported in the literature for grain size measurements of copper with individual additions of 0.05, 0.1, and 0.5 wt pct of Mo, In, Sn, Bi, Sb, Pb, and Se, cast under a protective atmosphere of pure Ar and water quenching. The columnar-to-equiaxed transition (CET) has been observed in copper, with an individual addition of 0.4B and with combined additions of 0.4Zr-0.04P and 0.4Zr-0.04P-0.015Ag and, in a previous study, with combined additions of 0.1Ag-0.069P (in wt pct). CETs in these B- and Zr-treated casts have been ascribed to changes in the morphology and chemistry of particles, concurrently in association with free solute type and availability. No further grain-refining action was observed due to microalloying additions of B, Mg, Ca, Zr, Ti, Mn, In, Fe, and Zn ( $\sim 0.1$  wt pct) with respect to DHP-Cu microalloyed with Ag, and therefore are no longer relevant for the casting conditions studied. The critical microalloying element for grain size control in deoxidized copper and in particular DHP-Cu is Ag.

DOI: 10.1007/s11661-016-3671-8

© The Author(s) 2016. This article is published with open access at Springerlink.com

## I. INTRODUCTION

IN early work, grain refinements of copper<sup>[1,2]</sup> and low alloy copper (which here refers to a maximum of 2 pct<sup>[1]</sup> and 2.6 pct<sup>[2]</sup>) were investigated *in air*. In the 1990s, grain refinement of copper was investigated under a protective atmosphere of *pure Ar* (99.997 pct), (enclosed chamber filled with Ar in a vacuum induction furnace, following vacuum purging).<sup>[3-6]</sup> Despite this demonstrable grain refinement of copper, exploitation of the beneficial solute additions was not on the whole applied to DHP-Cu with a view to becoming mainstream industrial practice. DHP-Cu is commercially pure copper (99.9 pct min. inclusive of 0.015 pct max. Ag), which has been deoxidized with P, leaving relatively high residual P in the range of 0.015-0.04 pct (all percentage compositions here are given in wt pct and ppm in wt ppm). DHP-Cu is one of the most common grades of copper and is a versatile material being used for engineering applications (nonelectric) such as sheet, plate, pipe, tube, and fittings.<sup>[7]</sup>

An as-cast fine-grain size structure in thin-walled DHP-Cu tube, for example, is important to reduce the susceptibility of crack propagation all the way across the tube wall thickness during the subsequent drawing and bending operations, ultimately resulting in rejection of the product.<sup>[8]</sup> It is also important to significantly improve the mechanical properties of both cast and

wrought products.<sup>[9,10]</sup> Hence, control of grain size in DHP-Cu is needed for an optimal combination of high component integrity, reduced component-processing costs, improved energy efficiency, and therefore reduced downstream CO<sub>2</sub> emissions, increasing the importance of economically attractive recyclable copper at the end of its life to avoid degrading quality.

DHP-Cu (99.9 pct min.) is obtained from copper cathode (99.9 pct min.-99.99 pct). During the electrolytic-refining process, copper cathodes are produced, whereby impurities are removed and valuables are recovered by separation. Ag, Au, and Pt are precious metals and are nobler than copper. They will be found as metals in the anode slime. More detail is given later, but a focal point has been to identify inoculant particles and solutes, which could be generated from commercially available copper-based master alloys, for grain structure control of copper and in particular DHP-Cu during solidification. The range includes master alloys such as copper-boron, copper-phosphorus, copper-zirconium, and copper-silver. Alternatively, by-product metals (Zn, In, Ag, *etc*) produced during the refining of copper<sup>[11]</sup> can potentially be used directly for the same purpose.

In this paper, taking as a starting point a brief overview of the work on the grain refinement of copper, we offer some broader reflections on the topic. The analysis is very much of an exploratory nature. We present new experimental evidence to highlight what appear to be under-researched aspects of the issues. First, the effects of individual additions of B, Mg, P, Ca, Zr, and Ti (generally 0.4 and 0.8 pct) on grain structure of copper have been investigated under TP-1 casting conditions.<sup>[12]</sup> Second, the corresponding combined effects of double solute additions (Cu-0.4X-P) for B,

---

MARÍA JOSÉ BALART and FENG GAO, Research Fellows, JAYESH B. PATEL, Senior Research Fellow, and ZHONGYUN FAN, Professor, Director of BCAST, are with the BCAST, Brunel University, Uxbridge, Middlesex, UB8 3PH, UK. Contact e-mails: mjbalarat@gmail.com, maria.balarat@brunel.ac.uk

Manuscript submitted September 24, 2015.

Mg, Ca, Zr, Ti, Ag, and Fe with P additions (low 0.03-0.04 pct) and/or high 0.15 pct) have also been assessed. Finally, the effects of additions of B, Mg, Ca, Zr, Ti, Sn, Ge, Mn, In, Ni, Fe, Zn, and Al (~0.1 wt pct) have been addressed with respect to DHP-Cu microalloyed with Ag.

## II. GRAIN REFINEMENT OF COPPER

### A. Previous Work on Grain Refinement of Copper

The earlier work by Northcott<sup>[1]</sup> on the grain refinements of copper and low alloy copper in air investigated the growth restriction of columnar grains in copper under unidirectional cooling, by small alloying additions, generally in the range from 0.1 to 2 pct, except for oxygen, in which the composition reported was in the range of ~0.005-0.1 pct. The length of the columnar grains in the axial direction (from the bottom of the ingot) was taken as a measure of the tendency of the investigated copper alloys to solidify in columnar form. The author proposed an empirical columnar growth restriction factor ( $G$ ) for different elemental additions into copper. This encompassed ordering the average values of columnar grain length and assigning corresponding values from 1 to 35. These  $G$  values are plotted in Figure 1(a), from which it can be seen that O, S, P, Ti, Ni, As, Se, Sn, Te, Pt, Tl, and Pb have comparatively higher  $G$  values. The elements were categorized in two groups: growth- and nongrowth-restricting elements having large ( $G \geq 13$ ) and small ( $G \leq 12$ )  $G$  values, respectively.<sup>[1]</sup> This is illustrated by the dashed line in Figure 1(a). Li particularly falls in the category of a nongrowth-restricting element. In contrast, the work of Gould *et al.*<sup>[2]</sup> showed evidence of a fine equiaxed grain structure after small additions of Li (0.02-0.07 pct), under casting conditions of a high degree of superheat at a casting temperature of 1422 K (1149 °C) in air.

In the 1990s, Bustos and Reif<sup>[3-6]</sup> investigated grain refinement of copper under an Ar atmosphere melting conditions, providing valuable information on grain characteristics (size, length, breadth, and percentage of equiaxed grains), which were measured on areas of equiaxed grains. The grain size measurement adopted by Bustos and Reif<sup>[3-6]</sup> was the linear intercept method on 15 vertical lines and 15 horizontal lines, although, no errors were estimated in their experimental report. In this work, grain size values from Reference 3 referred to the average grain size measured by the above linear intercept method. Occasionally, the corresponding percentage of equiaxed grains has also been reported here. The grain size values obtained for a constant solute addition of 0.1 pct to copper (99.99 pct purity), at an addition temperature of 1433 K (1160 °C), then held for 5 minutes, cast at 1433 K (1160 °C), and water quenched are depicted in Figure 1(b). These grain size values may be compared in Figure 1(b) with a grain size of 650  $\mu\text{m}$  for copper (99.99 pct purity) without additions (marked by the dashed line). This allows elemental additions having favorable and detrimental effects on grain size of copper to be discerned. When comparing

casting in air and under a protective atmosphere of pure Ar for the same binary system (Figure 1), there are some examples of binary systems, such as Cu-Zn and Cu-Ni systems, which had an opposite effect on grain growth restriction action.

One main issue is the grain boundary embrittlements of copper and its alloys caused by Bi, Te, S, Sn, O, Sb, Pb, Se, C, and in some cases P.<sup>[13-15]</sup> On the other hand, 'de-embrittling' elements, *i.e.*, elements that enhance grain boundary cohesion include Zr, Mg, B, Y, Ce, La, Ca, Nb, Li, U, and to a lesser extent P and Ti (see Reference 13 for details). This has been marked in Figure 1.

Grain refinement of copper has continued to be the aim of more recent investigations, and different solutions have focused on controlling microalloy compositions<sup>[16-18]</sup> and processing parameters.<sup>[8,9]</sup> In this work, characterizations of the influence of elemental additions on the grain structure of copper and DHP-Cu microalloyed with 150 ppm Ag have been carried out under TP-1 casting conditions.

Recently, the effects of additions of P and Ag as well as the de-embrittling elements of copper—B, Mg, Ca, Zr, and Ti—in concentrations of 0.085-0.5 pct, to provide some variations in contents within and outside of the DHP-Cu specification limits, without microalloying with Ag and cast at 1423 K (1150 °C) on the grain structure under TP-1 casting conditions have been reported elsewhere.<sup>[17]</sup> This temperature of 1423 K (1150 °C) was chosen because previous work on DHP-Cu reported in<sup>[16]</sup> showed that the macrostructure obtained at 1423 K (1150 °C) was mainly large, nonuniform columnar. Therefore, the potential beneficial effects of elemental additions on macrostructural changes could be observed at 1423 K (1150 °C). These results have been compared to those obtained after a nominal addition of 0.1 pct of B, Mg, Ca, Zr, and Ti to DHP-Cu with an addition of Ag of 0.015 pct and cast at 1403 K (1130 °C).<sup>[18]</sup> It was reported that, a nominal addition of 0.1 pct Ag to deoxidized copper gave the strongest grain-refining action at a casting temperature of 1423 K (1150 °C)<sup>[17]</sup> achieving CET. This necessitated phosphorus deoxidation of the copper melt resulting in a residual P level (0.039 pct). This finding has not previously been explicitly recognized in the field of grain refinement of copper. It was also reported that, a nominal addition of 150 ppm Ag to DHP-Cu gave the strongest grain-refining action at both casting temperatures of 1423 K (1150 °C)<sup>[16]</sup> and 1403 K (1130 °C)<sup>[18]</sup> achieving CET. It was therefore suggested making the maximum additions of P of 0.04 pct and of Ag of 0.015 pct to DHP-Cu for adequate grain size control.

CET is a microstructural transition which is characterized by the growth of equiaxed grains competing ahead of a columnar growth front during directional solidification.<sup>[19,20]</sup> Effective grain refinement requires not only the nucleating particles to be potent, efficient, sufficient in number, well dispersed, of suitable particles size, and of size distribution, but with even solidification under high undercooling conditions.<sup>[21]</sup> Another important factor controlling grain refinement is the type of solute, since solute elements can affect undercooling, the

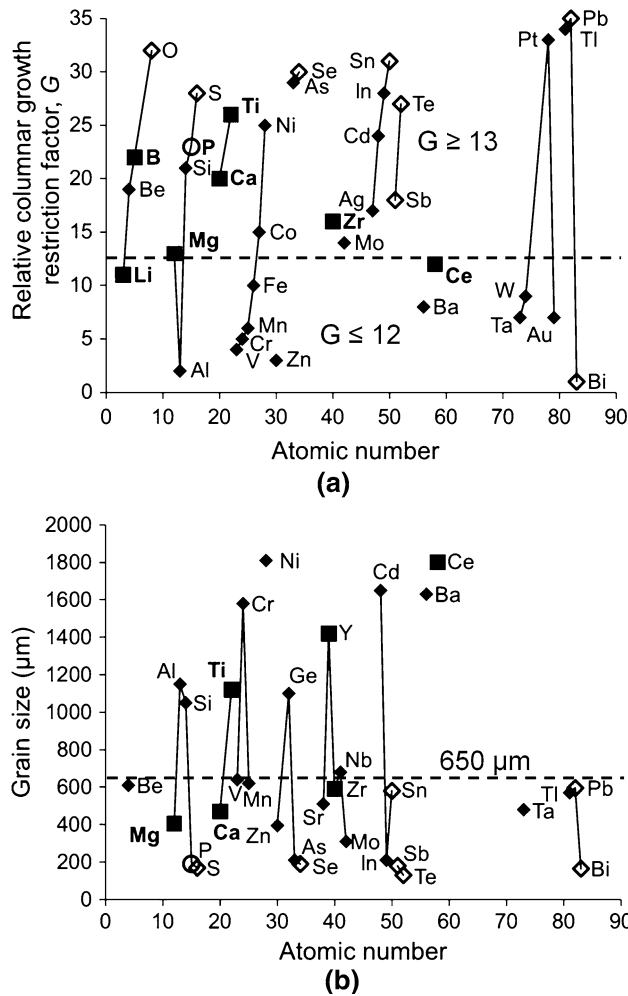


Fig. 1—(a) Variation of experimentally determined relative columnar growth restriction factor with elemental additions into copper rapidly cast in air (adapted from Ref. [1]): ~3.175 kg ingot castings, 76.2-mm diameter, and ~76.2-mm height; and (b) variation of copper grain size with 0.1 pct elemental additions into copper melt under an Ar atmosphere; the samples were cast at 1433 K (1160 °C) and water quenched (adapted from Ref. [3]): 220 g castings, 30-mm diameter, and 35-mm height; known grain boundary ‘embrittlers’ of copper are marked with unfilled symbols, and ‘de-embrittlers’ of copper are marked with filled square symbols and in bold (adapted from Ref. [13]), including the ambivalent character of phosphorus. Reprinted with permission from Ref. [17] copyright 2015, Taylor & Francis Ltd, [www.tandfonline.com](http://www.tandfonline.com).

nucleation potency of the liquid/nucleant interface and the grain growth restriction of a columnar front competing with equiaxed solidification.<sup>[22]</sup>

The comparative advantages of microalloying deoxidized copper and, in particular DHP-Cu, with 0.1 pct and 150 ppm Ag, respectively, are based on grain refinement of the as-cast structure, and increased strength levels<sup>[23]</sup> with a marginal decrease of both electric and thermal conductivities with respect to copper (99.99 pct purity) compared to a more detrimental effect of P. CET was also achieved at greater amounts of solute addition than 0.1 pct Ag. These are with a combined addition of 0.4Zr-0.039P and an individual addition of 0.5B (in wt pct).<sup>[17]</sup>

## B. Factors Controlling Secondary Dendrite Arm Spacing and Grain Size: Cooling Rate, Casting Temperature, Casting Atmosphere, Solute Type, and Solute Content

Casting temperature and atmosphere can have an influence on the grain refinement of copper.<sup>[5]</sup> Cooling rate (solidification time), type of solute (equilibrium distribution coefficient,  $k$ ) and amount of solute can also have an effect on secondary dendrite arm spacing<sup>[24]</sup> and grain structure<sup>[3,25]</sup> in copper.

Increasing the cooling rate leads to finer dendrite arm spacing.<sup>[24]</sup> For a given casting condition, the effect of cooling rate on the grain structure and percentage of equiaxed grains in copper is variable depending on the solute type.<sup>[3]</sup> In the case of copper (99.99 pct purity) under an Ar atmosphere, on decreasing the cooling rate resulting from using a water-cooled copper mold to a graphite mold, at a fixed casting temperature in the range of 1373 K to 1513 K (1100 °C to 1240 °C), the grain size values were increased.

Also, it provided quantitative measurement for the positive effect of decreasing the casting temperature at the two cooling rate conditions.<sup>[3]</sup> Plots of the variation of grain size with casting temperature for these conditions exhibited three stages: (i) 686-857 μm, 25-35 pct equiaxed grains, from 1433 K to 1513 K (1160 °C to 1240 °C); (ii) 343-629 μm, 25-35 pct equiaxed grains, from 1393 K to 1423 K (1120 °C to 1150 °C) and (iii) 229-243 μm, 57-74 pct equiaxed grains, from 1373 K to 1383 K (1100 °C to 1110 °C), under the water-cooled copper mold condition and (i) 1514-1771 μm, 10-20 pct equiaxed grains, from 1433 K to 1513 K (1160 °C to 1240 °C); (ii) 857-1371 μm, 10-20 pct equiaxed grains, from 1393 K to 1423 K (1120 °C to 1150 °C) and (iii) 686-771 μm, 10-20 pct equiaxed grains, from 1373 K to 1383 K (1100 °C to 1110 °C), under the graphite mold condition.

At constant and low solute additions, a finer dendritic structure was usually achieved in an alloy system having a low  $k$  value because the crystal growth surface is less stable than in those having a higher  $k$  value. In Cu-Ag alloys, increasing the Ag content for a given cooling rate and increasing the cooling rate for a given Ag content produced finer secondary dendrite arm spacing.<sup>[24,26]</sup> On decreasing the cooling rate resulting by changing from a water-cooled copper mold to a graphite mold, at a nominal solute addition of 0.1 wt pct into the copper melt under an Ar atmosphere and cast at 1433 K (1160 °C), Be, Mg, Ca, Sr, Al, Si, As, Sb, Bi, Se, and Te additions caused grain coarsening, whereas additions of In, Ti, Ge, Sn, Pb, P, S, and Se only resulted in a slightly increased grain size.<sup>[3]</sup> The type and content of solute and  $k$  effects on grain size are discussed below.

## C. The Growth Restriction Factor ( $Q$ )

The growth restriction factor  $Q$  has been used to evaluate quantitatively the role of solute in restricting crystal growth during solidification due to constitutional undercooling effects during solidification of dilute binary,<sup>[27-29]</sup> Eq. [1], and multicomponent alloy systems.<sup>[30]</sup>

$$Q = mc_o(k - 1) \quad [1]$$

where  $m$  is the slope of the liquidus,  $c_o$  is the solute concentration, and  $k$  is the equilibrium distribution coefficient.

In the case of Mg<sup>[27,28]</sup> and Al<sup>[29]</sup> alloys, a linear semi-empirical relationship between grain size ( $d$ ) and the reciprocal of  $Q$  has been determined, Eq. [2], which in turn relates the grain size to the solute content. Physically, the slope ( $b$ ) represents the potency of nucleant particles; the steeper the slope, the lower the potency, and the intercept ( $a$ ) corresponds to the number density of nucleant particles at infinite values of  $Q$ . For physical consistency, it should be the case that grain size > grain size (min.) > 0.

$$d = a + \frac{b}{Q} \quad [2]$$

where  $a$  and  $b$  are constants.

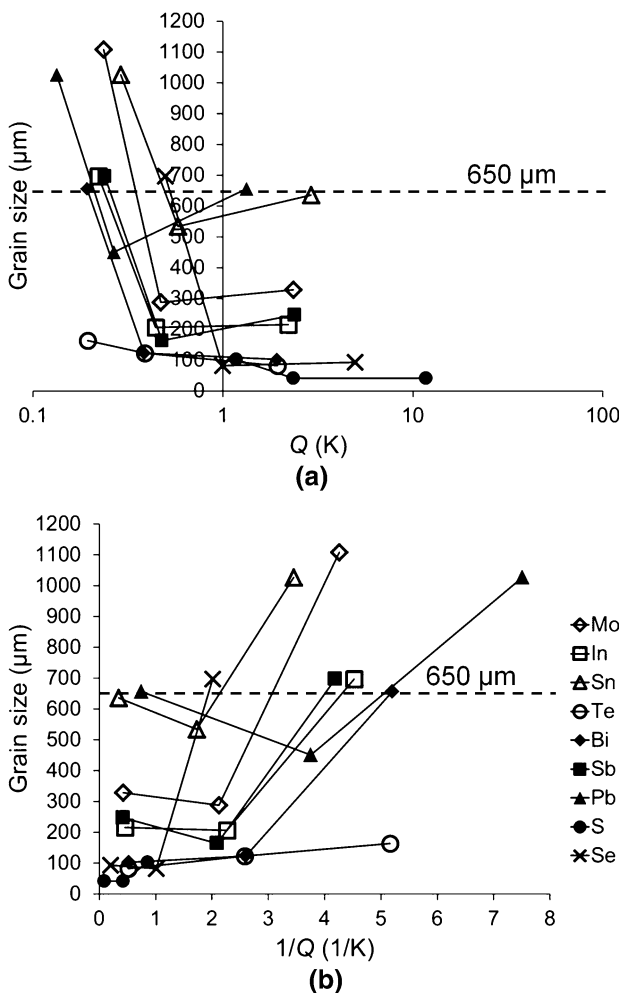


Fig. 2—Variation of grain size values from Bustos and Reif<sup>[3]</sup> with (a) growth restriction factor  $Q$  and (b) reciprocal of  $Q$  for different alloying elements. In comparison, the dashed lines correspond to a grain size of  $650 \mu\text{m}$ , which was that found in copper (99.99 pct purity) without additions.

In binary Mg alloys with Al, Ca, Zr, Si, and Zn, it has been demonstrated<sup>[27,28]</sup> that, on increasing the  $Q$  factor, the grain size decreased, and overall the grain size was smaller than that of the unrefined alloy. The decrease in grain size occurs in three stages: an initial stage with a large reduction in grain size with small solute additions, followed by a moderate second stage that continued until stabilization was reached.

The influence of increased amounts of solute additions (0.05, 0.1, and 0.5 pct) for a given solute type—Mo, In, Sn, Te, Bi, Sb, Pb, S, and Se—on the resulting grain size and the corresponding percentage of equiaxed grains in copper was also investigated by Bustos and Reif.<sup>[3]</sup> It was found that, in comparison to copper (99.99 pct purity) without additions, (i) Te and S additions produced in all three cases a significant grain-refining effect; in contrast, (ii) with an addition

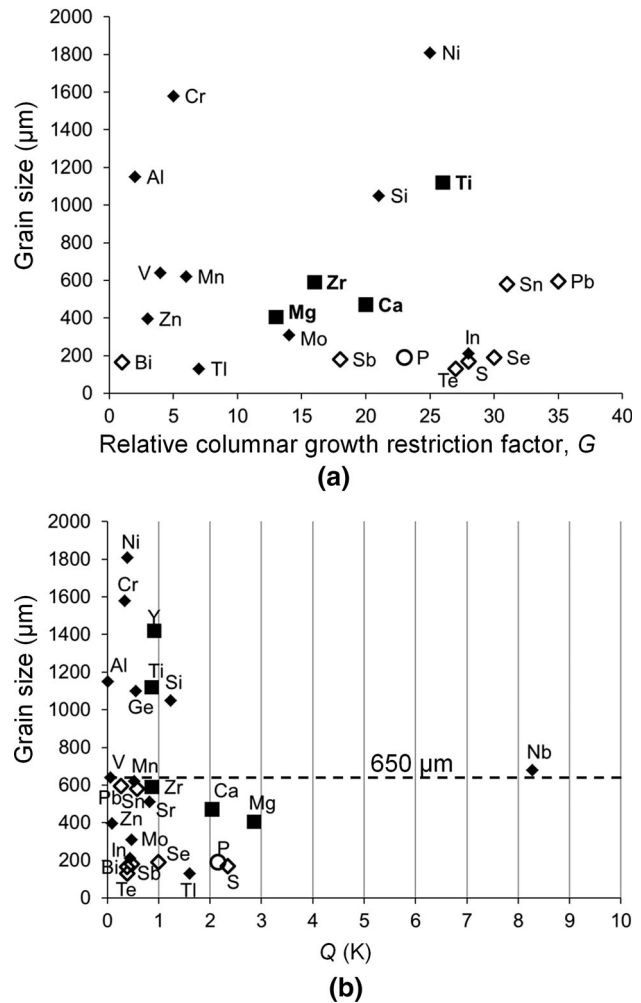


Fig. 3—Variation of grain size values from Bustos and Reif<sup>[3]</sup> with the growth restriction factors (a)  $G$  and (b)  $Q$  for an individual addition of 0.1 pct of different microalloying elements. In comparison, the dashed line corresponds to a grain size of  $650 \mu\text{m}$ , which was that found in copper (99.99 pct purity) without additions. Known grain boundary embrittlers of copper are marked with unfilled symbols, and ‘de-embrittlers’ of copper are marked with filled square symbols and in bold (adapted from Ref. 13), including ambivalent character of phosphorus.

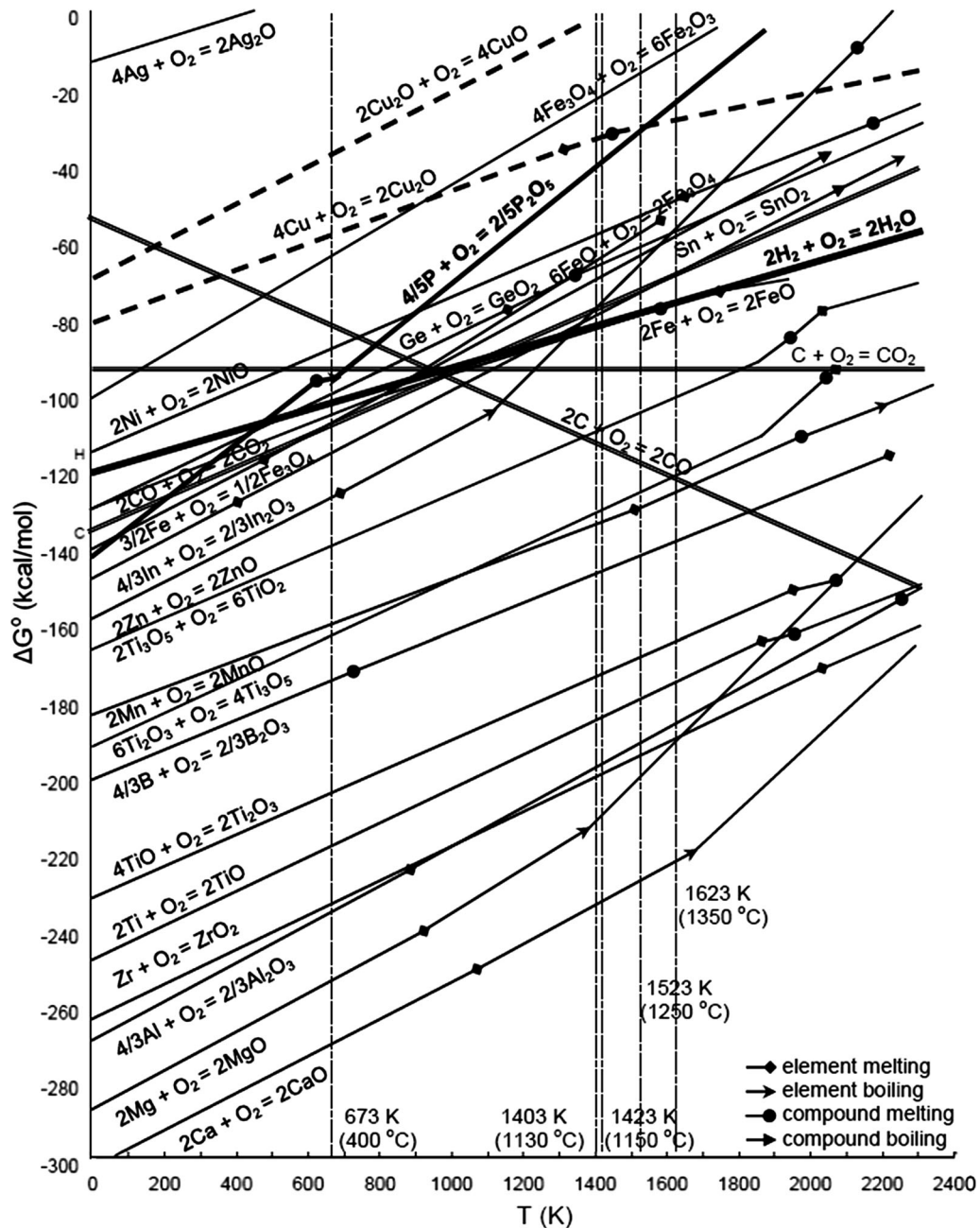


Fig. 4—Schematic of the Ellingham diagram for investigated oxides.<sup>[33,34]</sup> Note the reduction of CuO, Cu<sub>2</sub>O, NiO, and GeO<sub>2</sub> by hydrogen at above 673 K (400 °C). Adapted from Ref. [34] copyright (2006), reprinted with permission of Stanley M. Howard.

of 0.05 pct, the grain size increased significantly for Mo, Sn, and Pb; slightly for In, Sb, and Se; and marginally for Bi; (iii) a further addition of solute to 0.1 pct, however, resulted in a decrease in grain size; and (iv) with a further addition of solute to 0.5 pct, the grain sizes decreased slightly for Te and Bi; showed stabilization for S; although they increased for Sn, Sb, and Pb with respect to the 0.1 pct addition, these were, still marginal for Mo, In, and Se. These trends are echoed in Figures 2(a) and (b).

The trend of the variation of grain size with  $Q$  factor found in the copper samples containing an individual

addition of 0.05 pct of Mo, In, Sn, Bi, Sb, Pb, and Se (Figures 2(a) and (b)) was different from that after an individual addition of 0.05 pct of Te and S into copper reported above, and from the well-established evidence for binary Mg alloys with Al, Ca, Zr, Si and Zn in the initial stage, presented in References 27 and 28. As a result, the variation of grain size with  $1/Q$  factor is nonlinear (Figure 2(b)).

To summarize this section, as all these elemental additions in copper can affect grain size, and some of these elements are known embrittlers or de-embrittlers of copper and therefore can affect their performance.

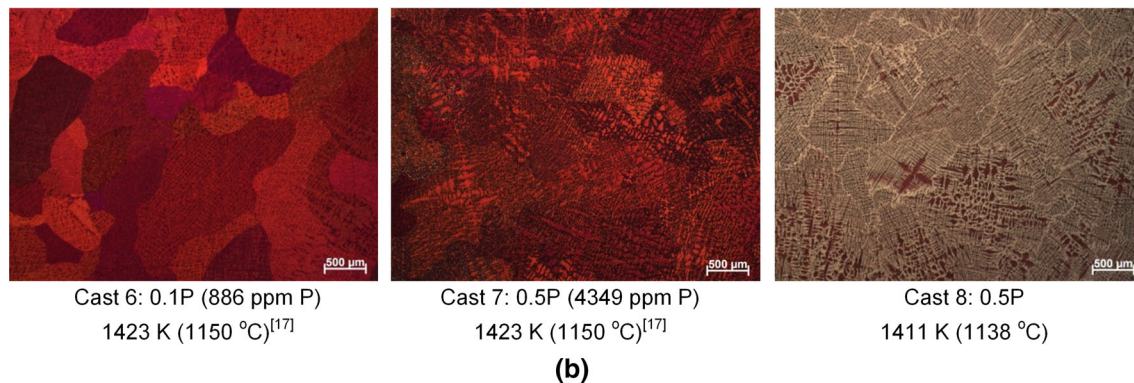
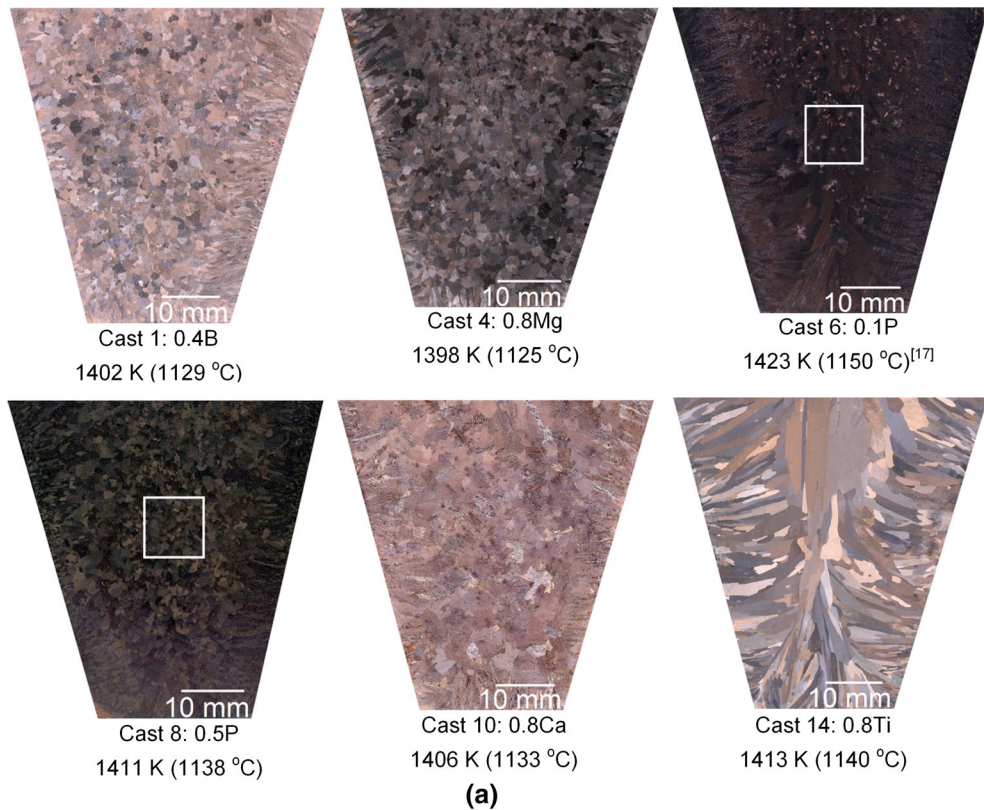


Fig. 5—(a) Macrographs of Cu-*X* alloys from Table II, and (b) optical micrographs of binary Cu-P alloys showing dendritic structure, polarized light microscopy. Casts 6 and 8 show details of region outlined by white squares in (a). Casting temperatures are shown for each TP-1 sample. Micrographs from casts 6 and 7 are reprinted with permission from Ref. [17], copyright 2015, Taylor & Francis Ltd, [www.tandfonline.com](http://www.tandfonline.com).

These elemental additions need to be controlled to produce stable inoculant particles in liquid copper phase, and also to have sufficient solute remaining to control grain size during solidification. Secondary dendrite arm spacing and grain size depend on the cooling rate, casting temperature, casting atmosphere, type, and content of the solute. For a given casting condition, the decreasing cooling rate increases the secondary dendrite arm spacing and grain size. The decreasing casting temperature produces grain refinement. At constant and low solute additions, a finer dendritic structure was usually achieved in an alloy system having a low *k* value. The type and content of solute present in copper is

therefore important in determining their effect on the grain size of copper. On the basis of empirical evidence reported in the literature for grain size measurements of copper with individual additions of 0.05, 0.1, and 0.5 wt pct of Mo, In, Sn, Bi, Sb, Pb, and Se, cast under a protective atmosphere of pure Ar and water quenching, some deviations exist in terms of the growth restriction factor (*Q*) framework. Further experiments are needed to confirm the influence of elemental additions on grain refinement of deoxidized copper, and in particular DHP-Cu, and this has been the aim of the present study in order to make further progress in the field of grain refinement of deoxidized copper.

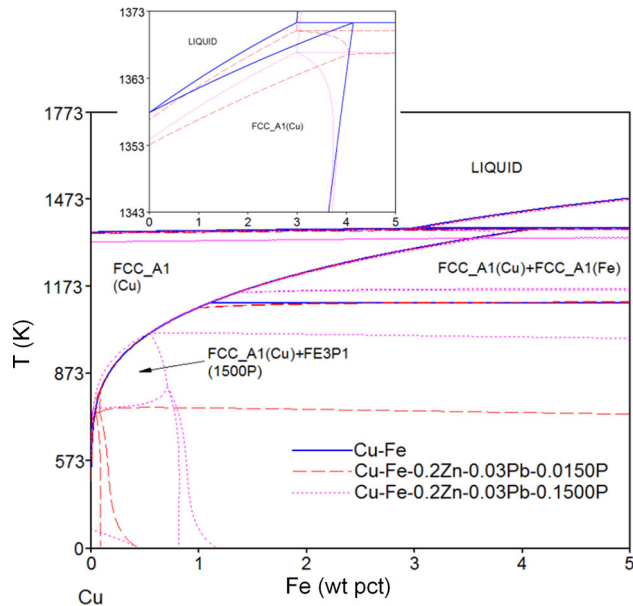


Fig. 6—Development of the Cu-rich region of the equilibrium phase diagram for the Cu-Fe alloy modified with 0.2 pct Zn, 0.03 pct Pb, 150 ppm P and 1500 ppm P (for interpretation of the references to color in this figure, the reader is referred to the web version of this article).

### III. EXPERIMENTAL

#### A. Materials

##### 1. High-purity copper cathode (Cu-CATH-1)

Copper grade A (Cu-CATH-1) was used in this study. Cu-CATH-1 is electrolytically refined to a purity of 99.95 pct, containing 0.04 pct maximum oxygen.<sup>[7]</sup> It has a maximum impurity content of 65 ppm and a maximum Ag content of 25 ppm, to conform to ASTM B115-10, GB/T 467-2010, and BS EN 1978:1998.

##### 2. DHP-Cu

DHP-Cu is virtually oxygen free 10 ppm maximum and has a minimum commercial purity of 99.9 pct inclusive of 0.015 pct maximum Ag.<sup>[7]</sup> It is susceptible to having an impurity content of 65 ppm maximum inherited from its precursor material Cu-CATH-1. It has a maximum content of P of 0.04 pct and a maximum content of C of 1.9 ppm. Note the very low solubility of C in liquid Cu near the melting point of Cu.<sup>[31]</sup> According to the peritectic type Cu-C equilibrium phase diagram which was proposed in Reference 31, the value of the solubility of C in copper is 10 at ppm (1.9 wt ppm) at 1373 K (1100 °C). The total master alloy and metallic additions could change up to upper bound values between 0.0523 and 0.0850 pct (corresponding to maximum  $[1000 - (10(O) + 65(\text{impurities}) + 400(P) + 1.9(C)) = 523 \text{ ppm}]$  and minimum  $[1000 - (0(O) + 0(\text{impurities}) + 150(P) + 0(C)) = 850 \text{ ppm}]$  composition values carried over to ensure the composition is within required limits. To convert the Cu-CATH-1 melt into DHP-Cu, the melt was first deoxidized with graphite flake.

#### 3. Alloying additions

Details of the commercially available copper master alloys and materials used in the present investigation as well as of all the experiments are given in Tables II through V. Note that deliberate microalloying additions to DHP-Cu were increased to enhance solute effects, ultimately to justify potential microalloying additions.

#### B. Castings

For each experiment in air, 1 kg of Cu-CATH-1 was remelted at ~1473 K (1200 °C) in a clay-graphite crucible in an induction furnace in air using graphite flake protection on the surface of the melt for deoxidation during melting. Elemental additions as detailed in Tables II through V were wrapped in copper foil and were generally made at 1473 K (1200 °C) and at the same time (when more than one addition was made). Master alloys with higher melting point, such as Cu-10.2Fe, necessitated higher melting temperatures (1623 K (1350 °C) max.). Additions were made just before casting using a graphite plunger. The melt was always stirred using a graphite rod during the additions and just before pouring into a standard TP-1 mold<sup>[12]</sup> preheated to 523 K (250 °C), followed by rapidly transferring into the water tank stand where a constant cooling rate of 3.5 K/s was maintained at the center of a cross section located 38 mm from the base of the TP-1 sample. The temperature was monitored using a type K (nickel chromium vs nickel aluminum) thermocouple to a temperature control of  $\pm 2.2$  K. In particular, when making an addition of 0.4 pct B into the copper melt in the form of Cu-1.73B master alloy, the B-containing copper melt was exposed for a longer time to graphite (clay-graphite crucible and graphite flake protection), thereby allowing the possible formation of B<sub>4</sub>C phase.

#### C. Characterization Techniques

##### 1. Macroscopic examination

The TP-1 casting from each experiment was sectioned longitudinally parallel to its axis. In order to reveal the grain structure, samples were ground and macro-etched using a 1:1 vol. solution of HNO<sub>3</sub> and H<sub>2</sub>O.

##### 2. Optical microscopy

Longitudinal sections were taken from the center of selected TP-1 samples at 28-38 mm from the base, mounted in Bakelite, ground, and polished prior to etching in a solution of 25 mL distilled water, 25 mL ammonia water, and 0.5 mL H<sub>2</sub>O<sub>2</sub> (27 pct w/w), and were examined under optical microscopy.

##### 3. ICP analysis

Samples (1 cm<sup>3</sup>) were also located in the mid-section 28-38 mm from the base of selected TP-1 samples and were analyzed by inductively coupled plasma optical emission spectrometry (ICP-OES).

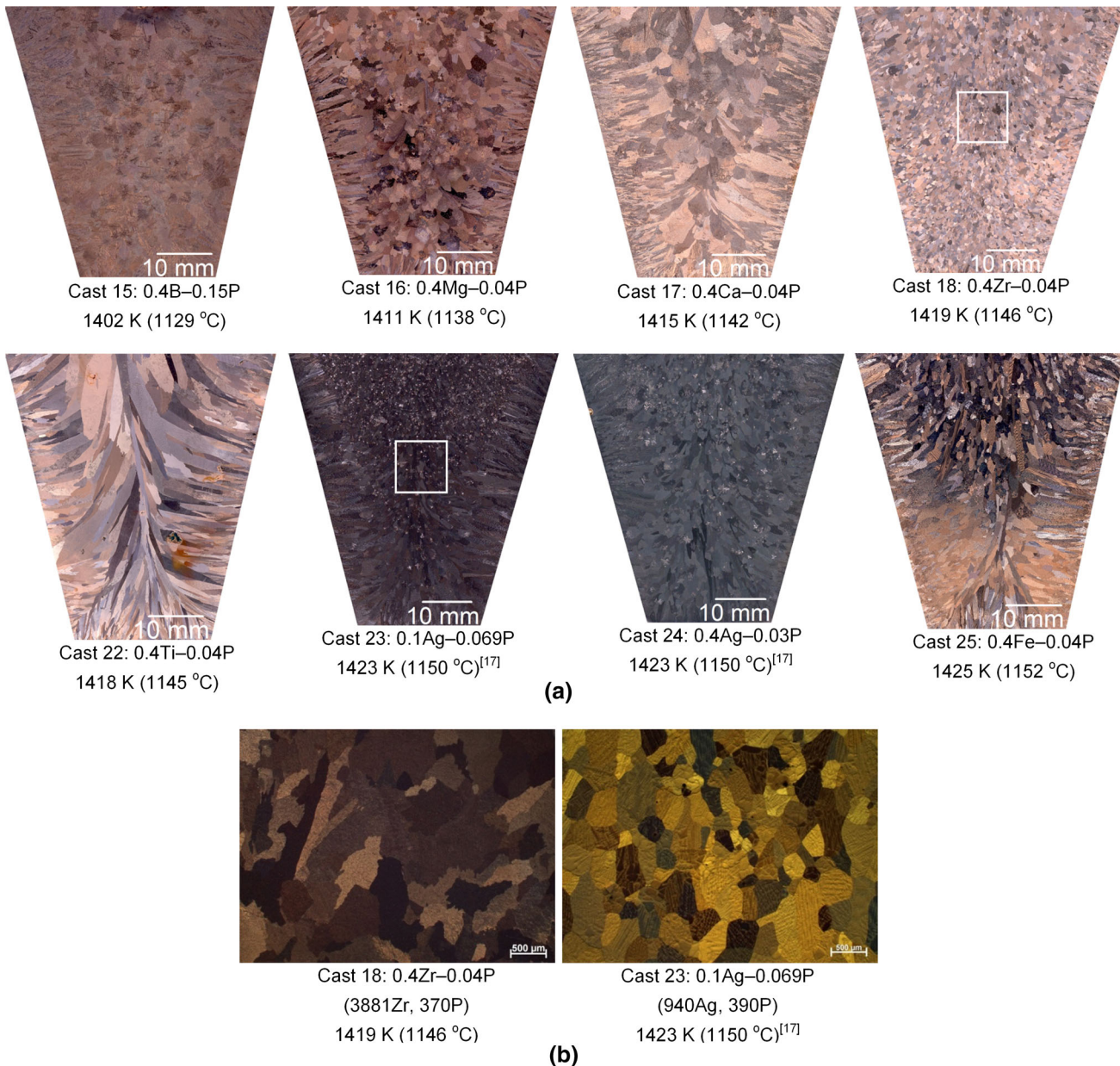


Fig. 7—(a) Macrographs of Cu-X-P alloys from Table III, and (b) detail of region outlined by white squares, polarized light microscopy. Casting temperatures are shown for each TP-I sample. Images from casts 23 and 24 are reprinted with permission from Ref. [17], copyright 2015, Taylor & Francis Ltd, [www.tandfonline.com](http://www.tandfonline.com).

#### 4. SEM

Optical specimens were examined in the unetched state in a Zeiss Supra 35VP field emission gun (FEG)-SEM operating at 5 and 25 kV and equipped with energy dispersive X-ray spectroscopy (EDS) system fitted with a silicon drift detector. Imaging was obtained under secondary electron (SE) and backscattered electron (BSE) modes. A total of about 75 spectra were collected from matrix, particles and different regions within the particle. EDS qualitative microanalysis was processed using Oxford-INCA microanalysis software. C and O contents were assessed after spectra normalization of the C K and O K peaks to the Cu L peak, respectively, and operating at 5 kV.<sup>[32]</sup> Qualitative

assessment of the P, B, and Zr contents was determined accordingly as the ratio of peak intensities P K to B K (operating at 5 kV) and P K to Zr L (operating at 25 kV) after peak deconvolution.

## IV. RESULTS AND DISCUSSION

### A. *Q* Factor

The Cu-rich regions of the equilibrium phase diagrams for binary Cu-X, ternary Cu-X-300P, and quaternary Cu-X-300P-150Ag and Cu-X-400P-150Ag systems, and their magnified regions (small insets) were



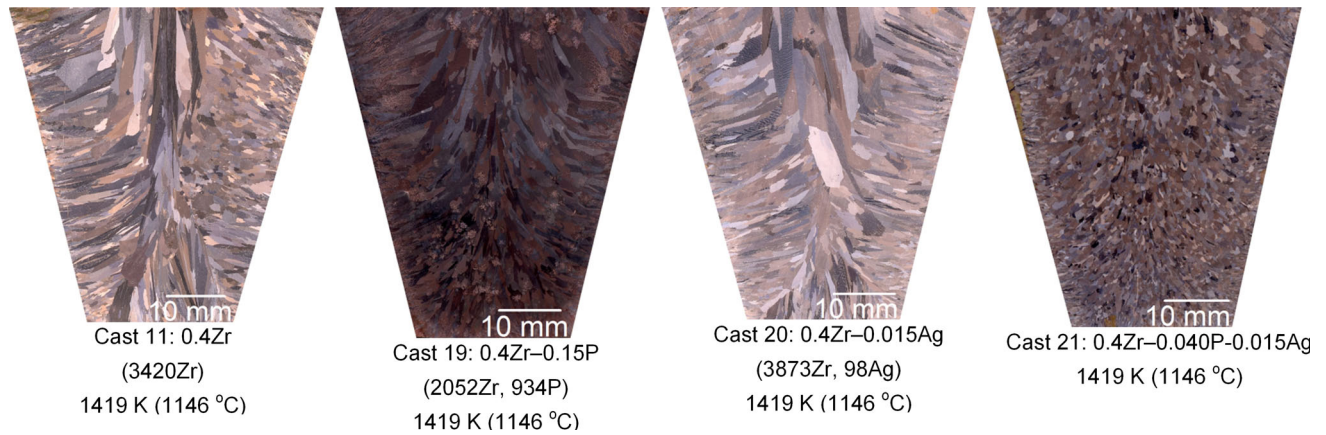


Fig. 8—Macrographs of Cu-0.4Zr, Cu-0.4Zr-0.15P, Cu-0.4Zr-0.015Ag, and Cu-0.4Zr-0.04P-0.015Ag alloys. Casting temperatures are shown for each TP-1 sample.

plotted, some of which are reproduced in Figure A1 in the Appendix.

We have determined  $m$  and  $k$  values using binary phase diagrams, to calculate the growth restriction parameter values,  $m(k - 1)$ , from Eq. [1] for various alloying elements in copper. These values are given in Table I, together with superheat changes with respect to 1433 K (1160 °C) due to 0.1 pct microalloying additions for binary Cu- $X$  systems. As seen from Table I, Nb has the highest growth restriction parameter value,  $m(k - 1)$ , followed in decreasing order by B > O > Mg > S > P > Ca > Zr > Ti. In the aforementioned study<sup>[3]</sup> on the effect of solute elements on grain refinement of copper under a protective atmosphere of pure Ar, grain size measurements were reported for a constant solute addition of 0.1 pct, at a casting temperature of 1433 K (1160 °C), followed by water quenching. Those grain size values of Reference 3 are plotted against the corresponding G values given in Reference 1 in Figure 3(a) and also against the corresponding calculated Q values using Eq. [1] in Figure 3(b).

The scatter-plot in Figure 3(a) shows the lack of correlation between grain size and G values. Since similar Q values should be expected to give similar grain size values under the same casting conditions and the same nucleant particle populations, independently of the alloy system, and so higher Q values would be expected to yield finer grains. However, as can be seen in Figure 3(b), there is a large variation in grain size values at different intervals of Q values, namely 0-1, 1-2, and 2-3. Overall, on increasing the intervals of Q values from 0-1 to 1-2 and to 2-3, the upper bound values of the grain sizes decreased, and the scatter bands narrowed in ranges: 130-1810  $\mu\text{m}$  for 0-1; 130-1050  $\mu\text{m}$  for 1-2, and 169-470  $\mu\text{m}$  for 2-3.

In comparison, an overall similar trend has previously been observed for Mg alloys.<sup>[27,28]</sup> Those results were explained by deviations due to inclusion populations that may be introduced into the Mg melt with the solute additions, variations in particle populations due to Mg reactivity and superheat modification with alloying. However, the base materials used in Reference 3 were copper (99.99 pct purity) and elemental additions (99.99

pct purity). Furthermore, marginally small differences in superheat changes due to 0.1 pct microalloying additions, as determined in Table I are not sufficient to account for this large variation in grain size values. This is indicative of the solute type effect *per se* as originally suggested by Northcott.<sup>[1]</sup> Another example of this is shown in Figure 3(b), where despite the highest Q value of 8.269 was obtained with 0.1 pct Nb, its grain size value remained practically unchanged (680  $\mu\text{m}$  with a Nb addition cf. 650  $\mu\text{m}$  without a Nb addition).

It is of interest to note that an addition of Mo of 0.1 pct to copper (99.99 pct purity) resulted in efficient grain refinement (310  $\mu\text{m}$ ), although with a limited percentage of equiaxed grains (47 pct).<sup>[3]</sup> According to the calculated Cu-rich region of the equilibrium phase diagram of peritectic type for the Cu-Mo system (Figure A1(p)), 0.1 pct Mo is slightly below the invariant point 0.1076 pct Mo at 1357.38 K (1084.23 °C), and the solidification range at 0.1 pct Mo is only 0.0326 K.

### B. Melt Deoxidation

The copper melt was protected from oxidation by covering with graphite flake. Additions of P in the form of Cu-15P master alloy were made before casting to deoxidize the melt during pouring. An *Ellingham diagram*<sup>[33,34]</sup> for oxides of alloying additions investigated is depicted in Figure 4. In comparison to Ag and P, the rest of alloying additions have higher affinity to oxygen, and in turn, could preferably oxidize in the presence of P when exposed to an oxygen-containing atmosphere at high melting temperatures. It can also be seen from Figure 4 that CuO, Cu<sub>2</sub>O, NiO and GeO<sub>2</sub> can correspondingly be reduced to Cu, Ni and Ge by using H<sub>2</sub> as a reductant above 673 K (400 °C) (H<sub>2</sub> embrittlement reaction). Hence, oxides which can be reduced by H<sub>2</sub> should not be introduced in the copper melt. Similarly, at higher temperatures, In<sub>2</sub>O<sub>3</sub> and FeO can be reduced by carbon to In (>1050 K (777 °C) approx.) and Fe (>1000 K (727 °C) approx.), respectively. Mn, B, Ti, Zr, Al, Mg, and Ca plots do not cross the carbon plot at feasible melting temperatures used in the present investigation, *i.e.* from ~1473 K to 1523 K (1200 °C to

**Table I. Liquidus Slope ( $m$ ), Equilibrium Distribution Coefficient ( $k$ ), Growth Restriction Parameter  $m(k - 1)$ , Liquidus ( $T_l$ ), and Solidus ( $T_s$ ) Temperatures, and Superheat for Alloying Elements (0.1 pct) in Copper at 1433 K (1160 °C)**

	$m$	$k$	$m(k - 1)$	Invariant reactions and characteristics at the Cu-rich region	$T_l$ [K (°C)] at 0.1 pct	$T_s$ [K (°C)] at 0.1 pct	$\Delta T$ (K) at 0.1 pct	Superheat (K) at 0.1 pct 1433 K (1160 °C)
Nb	25.70	4.218	82.69	peritectic	1360.31 (1087.16)	1358.38 (1085.23)	1.93	73
B	-56.23	0.098	50.74	eutectic	1351.77 (1078.62)	1287.73 (1014.58)	64.04	81
O <sup>[42]</sup>	-41.86	0.017	41.13	eutectic / monotectic	1351.81 (1078.66)	1338.00 (1064.85)	13.81	81
Mg	-30.90	0.075	28.58	eutectic	1354.79 (1081.64)	1322.67 (1049.52)	32.12	78
S <sup>[34,42]</sup>	-23.83	0.016	23.44	eutectic	1355.60 (1082.45)	1340.00 (1066.85)	15.60	78
P	-23.73	0.092	21.55	eutectic, congruent	1355.09 (1081.94)	1336.17 (1063.02)	18.92	78
Ca	-20.38	0	20.38	eutectic	1356.43 (1083.28)	1182.82 (909.67)	173.61	77
Tl	-16.76	0.045	16.00	monotectic	1357.53 (1084.38)	1348.07 (1074.92)	9.46	76
Si	-19.80	0.376	12.35	peritectic	1356.24 (1083.09)	1353.19 (1080.04)	3.05	77
Se <sup>[24]</sup>	-9.94	0	9.94	monotectic	1357.06 (1083.91)	1336.15 (1063.00)	20.91	76
Y	-9.13	0	9.13	eutectic	1356.85 (1083.70)	1153.41 (880.26)	203.44	76
Zr	-8.70	0	8.70	eutectic	1356.85 (1083.70)	1284.77 (1011.62)	72.08	76
Ti	-11.70	0.264	8.61	intermediate solid solution phases / compounds	1356.57 (1083.42)	1353.07 (1079.92)	3.50	77
Sr	-8.23	0	8.23	intermediate compounds	1356.95 (1083.80)	1118.35 (845.20)	238.6	77
Sn	-6.20	0.064	5.80	peritectic	1357.13 (1083.98)	1348.63 (1075.48)	8.50	76
Ge	-8.00	0.310	5.52	intermediate solid solution phases	1357.04 (1083.89)	1355.39 (1082.24)	1.65	76
Mn	-8.68	0.397	5.23	miscibility gap in the solid state	1356.90 (1083.75)	1355.55 (1082.40)	1.35	76
Sb	-5.56	0.141	4.78	eutectic, congruent	1357.20 (1084.05)	1353.98 (1080.83)	3.22	76
Mo	-6.02	0.218	4.71	peritectic	1357.42 (1084.27)	1357.38 (1084.23)	0.04	76
In	-5.55	0.203	4.42	peritectic	1357.24 (1084.09)	1355.14 (1081.99)	2.10	76
Ni	6.75	1.57	3.88	isomorphous	1358.70 (1085.55)	1358.46 (1085.31)	0.24	74
Te <sup>[43]</sup>	-3.88	0	3.88	monotectic	1357.61 (1084.46)	1325.00 (1051.85)	32.61	76
Bi	-3.85	0	3.85	very low solubility of Bi in Cu	1356.77 (1083.62)	1272.18 (999.03)	84.59	76
Ag	-4.95	0.261	3.66	eutectic	1357.28 (1084.13)	1355.97 (1082.82)	1.31	76
Cr	-6.54	0.489	3.34	eutectic	1357.09 (1083.94)	1356.46 (1083.31)	0.63	76
Pb	-3.07	0.133	2.66	monotectic	1357.71 (1084.56)	1355.73 (1082.58)	1.98	75
Fe	5.15	1.447	2.30	peritectic	1358.55 (1085.40)	1358.40 (1085.25)	0.15	75
Au	-1.93	0.487	0.99	miscibility gap in the solid state	1357.58 (1084.43)	1357.36 (1084.21)	0.22	76
Zn	-3.35	0.722	0.93	peritectic	1357.69 (1084.54)	1357.56 (1084.41)	0.13	75
Pt	1.83	1.500	0.92	miscibility gap in the solid state	1358.11 (1084.96)	1357.95 (1084.80)	0.16	75
V	2.96	1.214	0.63	peritectic	1358.06 (1084.91)	1358.01 (1084.86)	0.05	75
Al	0.81	1.138	0.11	intermediate solid solution phases	1358.21 (1085.06)	1358.19 (1085.04)	0.02	75

Table II. Cu-X Alloys Investigated

Cast	Casting T [K (°C)]	Nominal Compositions (Wt Pet)	T <sub>1</sub> [K (°C)]	T <sub>s</sub> [K (°C)]	ΔT (K)	Master alloys/materials (Wt Pet)	Macrostructure
1 B	1402 (1129)	0.4	1337.00 (1063.85)	1287.34 (1014.19)	49.66	Cu-1.73B-0.04Si- 0.01Fe-0.01Sn-0.005Pb	CET
2 O <sup>[16]</sup>	1423 (1150)	(1590 wt ppm) copper cathode 0.4	1349.34 (1076.19)	1338.00 (1064.85)	11.34		CET
3 Mg	1411 (1138)		1346.12 (1072.96)	1248.64 (975.49)	97.48	Cu-20Mg	CET excessive equiaxed grain coarsening
4	1398 (1125)	0.8	1332.87 (1059.72)	1179.28 (906.13)	153.59		CET
5	1372 (1099)	1.6	1306.28 (1033.13)	1088.18 (815.03)	218.10		CET
6 P <sup>[17]</sup>	1423 (1150)	0.1 (886 wt ppm)	1355.09 (1081.94)	1336.17 (1063.02)	18.92	Cu-15P	CET to a lesser extent
7 <sup>[17]</sup>	1423 (1150)	0.5 (4349 wt ppm)	1346.11 (1072.96)	1245.05 (971.90)	101.06		CET excessive equiaxed grain coarsening
8	1411 (1138)	0.5	1346.11 (1072.96)	1245.05 (971.90)	101.06		CET
9 Ca	1415 (1142)	0.4	1349.53 (1076.38)	1182.81 (909.66)	166.72	Cu-6.87Ca-0.005Al- 0.001Fe-0.001Mg	CET excessive equiaxed grain coarsening
10	1406 (1133)	0.8	1341.06 (1067.91)	1182.12 (908.97)	158.94		CET excessive equiaxed grain coarsening
11 Zr	1419 (1146)	0.4	1354.16 (1081.01)	1240.59 (967.44)	113.57	Cu-9.28Zr-0.11Sn- 0.09Fe-0.002Pb	large columnar/some equiaxed grains
12	1416 (1143)	0.8	1350.41 (1077.26)	1240.59 (967.44)	109.82		large columnar
13 Ti	1418 (1145)	0.4	1353.18 (1080.03)	1339.08 (1065.93)	14.10	Cu-28.924Ti-0.045Fe- 0.01max.Ni-0.002Pb	large columnar
14	1413 (1140)	0.8	1348.18 (1075.03)	1322.09 (1048.94)	26.09		large columnar

\*Casting temperature to keep a constant degree of superheat of 1423 – 1357.77 K (1150 – 1084.62 °C), except for the nondeoxidized Cu-CATH-1 and deoxidized 0.1-0.5 pct P cast at 1423 K (1150 °C).

Casts 2, 6, and 7 are reprinted with permission from Ref. [16], copyright 2015, Taylor & Francis Ltd, [www.tandfonline.com](http://www.tandfonline.com).

**Table III. Cu-X-P, Cu-0.4Zr-0.015Ag, and Cu-0.4Zr-0.04P-0.015Ag Alloys Investigated**

Cast		Casting T** [K (°C)]	Nominal Compositions (wt pct)	ICP-OES Trace Analysis (wt ppm)	Macrostructure
15	B + P	1402 (1129)	0.4B, 0.15P		CET excessive equiaxed grain coarsening
16	Mg + P	1411 (1138)	0.4Mg, 0.04P		CET excessive equiaxed grain coarsening
17	Ca + P	1415 (1142)	0.4Ca, 0.04P		CET excessive equiaxed grain coarsening
11	Zr*	1419 (1146)	0.4Zr	3420Zr, 6Pb, 69Fe, 51Sn	large columnar/some equiaxed grains
18***	Zr + P	1419 (1146)	0.4Zr, 0.04P	3881Zr, 370P, 70Fe, 5Sn	CET
19	Zr + P	1419 (1146)	0.4Zr, 0.15P	2052Zr, 934P, 121Fe, 51Sn	columnar
20	Zr + Ag	1419 (1146)	0.4Zr, 0.015Ag	3873Zr, 98Ag	large columnar
21	Zr + P + Ag	1419 (1146)	0.4Zr, 0.04P, 0.015Ag		CET
22	Ti + P	1418 (1145)	0.4Ti, 0.04P		large columnar
23***	Ag + P <sup>[17]</sup>	1423 (1150)	0.1Ag, 0.069P	940Ag, 390P	CET
24	Ag + P <sup>[17]</sup>	1423 (1150)	0.4Ag, 0.03P		CET to a lesser extent
25	Fe + P	1425 (1152)	0.4Fe, 0.04P		columnar

\*Zr casting from Table II is given for comparison.

\*\*Casting temperature to keep a constant degree of superheat of 1423 – 1357.77 K (1150 – 1084.62 °C), except for cast 24 at 1423 K (1150 °C) (1421 K (1148 °C) for a constant superheat).

\*\*\*Casts 18 and 23 were cast twice to confirm the macrostructure.

Casts 23 and 24 are reprinted with permission from Ref. 17, copyright 2015, Taylor & Francis Ltd, [www.tandfonline.com](http://www.tandfonline.com).

1250 °C). Note that, C, P, B, Li, and Mg are industrially effective deoxidizers of copper alloy melts, the reaction products being CO / CO<sub>2</sub>, P<sub>2</sub>O<sub>5</sub> / 2Cu<sub>2</sub>O.P<sub>2</sub>O<sub>5</sub>, B<sub>2</sub>O<sub>3</sub>, Li<sub>2</sub>O, and MgO, respectively.<sup>[24]</sup>

Those solute elements can react in the copper melt to form oxides in an oxygen-containing atmosphere; phosphides such as BP, Mg<sub>3</sub>P<sub>2</sub>, Ca<sub>3</sub>P<sub>2</sub>, TiP, ZrP<sub>2</sub>, AlP, Ni<sub>2</sub>P, Fe<sub>2</sub>P, Fe<sub>3</sub>P, MnP, Mn<sub>2</sub>P, Zn<sub>3</sub>P<sub>2</sub>, etc. and carbides such as B<sub>4</sub>C, CaC<sub>2</sub>, TiC, ZrC, Fe<sub>3</sub>C, Mn<sub>3</sub>C, MoC, Mo<sub>2</sub>C, etc. in the presence of P and C, respectively<sup>[35,36]</sup> (for the later, as cited in Reference 37) and even mixed ternary Fe-Cu-P intermetallic particles,<sup>[38]</sup> and Cu<sub>2</sub>ZrP<sub>2</sub> and ZrP<sub>2</sub>O<sub>7</sub> phases.<sup>[39]</sup>

In the case of solute reaction, the restriction factor as a measure of the effect of solute on grain refinement can only be calculated using thermodynamic packages.<sup>[27–30]</sup> It was therefore of interest to assess first the as-cast grain structure of copper with single additions of B, Mg, P, Ca, Zr, and Ti in the form of master alloys (Table II) under the combined effects of possible formation of endogenous particles in the Cu melt as a result of their reaction with carbon and/or oxygen and their possibility of acting as substrate for heterogeneous nucleation of copper grains. Details of the resulting macrostructures are given in the last column of Table II, with some examples illustrated in Figure 5. In particular, a micrograph for cast 8 of 0.5 pct P at 1411 K (1138 °C) is shown in Figure 5(b) to compare with cast 6 (0.1 pct P) and cast 7 (0.5 pct P), both at 1423 K (1150 °C).<sup>[17]</sup> On decreasing the casting temperature from 1423 K to 1411 K (1150 °C to 1138 °C) for a given addition of 0.5 pct P, the degree of CET increased, which is as expected. Comparing 0.1 and 0.5 pct P additions at 1423 K (1150 °C), grain coarsening was observed with the increase of the P addition to 0.5 pct.

### C. Phosphide Particles

The work of Gould *et al.*<sup>[2]</sup> reported a fine equiaxed microstructure (130 μm) after an addition of 2.42 pct Fe to electrolytic copper (99.883 pct), under casting conditions of a high degree of superheat at a casting temperature of 1422 K (1148.9 °C) in air. This was attributed to a peritectic solidification mechanism. However, 2.42 pct Fe is below the invariant point 2.99 pct Fe at 1371.35 K (1098.35 °C) (Figure A1(m)). Hence, the observed grain-refining effect at 2.42 pct Fe addition may instead be caused by constitutional undercooling. Furthermore, a columnar macrostructure after Fe additions in the range of 0.02-1.32 pct is reported.

Structural characterization by TEM<sup>[40]</sup> in a Cu-1Fe alloy identified rod-shaped α-Fe particles and by SEM<sup>[38]</sup> and TEM<sup>[41]</sup> in the bulk of a CuFe<sub>2</sub>P alloy (97.0min.Cu—2.1-2.6Fe—0.05-0.20Zn—0.03-max.Pb—0.015-0.15P—0.2max.others (wt pct)) reported also iron-containing intermetallic particles. The CuFe<sub>2</sub>P alloys of Reference 41 had P contents in the base compositions of 0.065 and 0.053 pct. Iron-containing intermetallic particles were observed to be globular with particle size ranging from <1 μm up to 10 μm, coarse plate-like or irregular morphology up to 5 μm in size.<sup>[38,41]</sup> The presence of ternary Fe-Cu-P intermetallic particles would not be initially expected in the liquid region, according to the thermodynamic analysis (Figure 6).<sup>[38]</sup>

A second point of interest was therefore to investigate the as-cast grain structure of copper under the combined effects of double solute additions (Cu-0.4X-P) for B, Mg, Ca, Zr, Ti, Ag, and Fe with P additions (low (0.03-0.04 pct) and/or high 0.15 pct) as reported in Reference 38. Details of the resulting macrostructures are given in the last column in Table III, with some

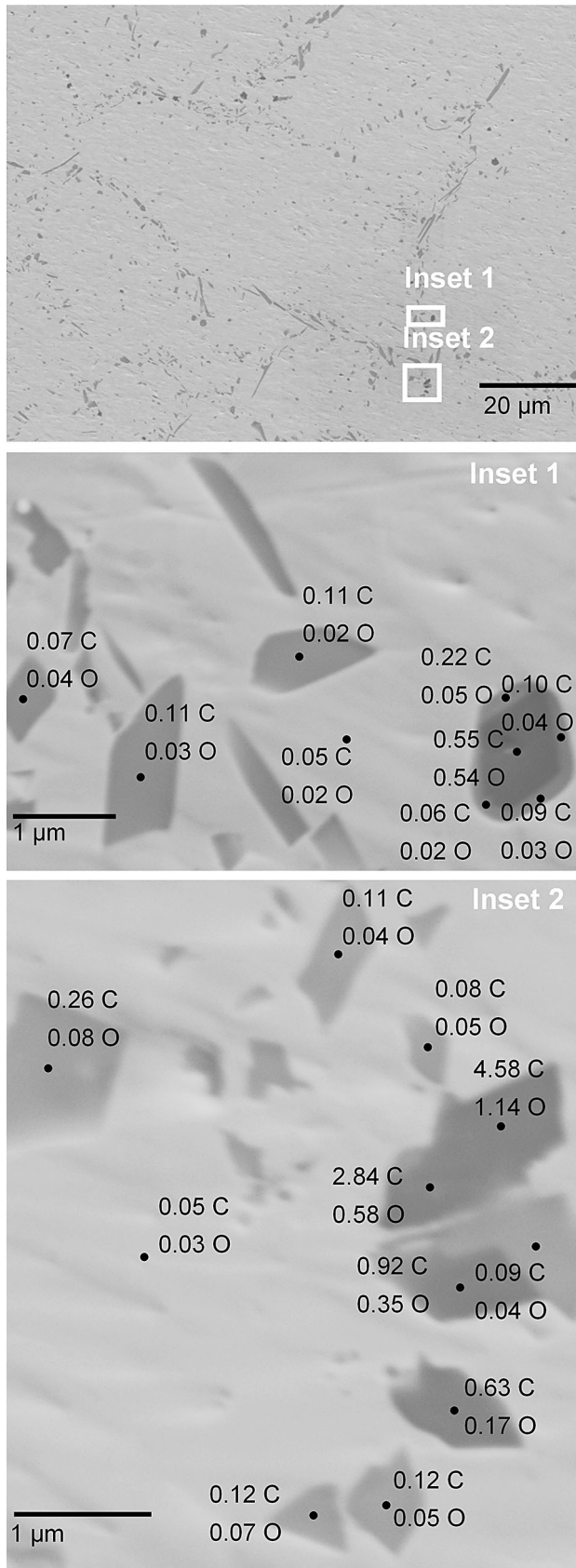


Fig. 9—SE micrographs of B-containing particles from cast 1 of 0.4B. C and O values represent normalized net intensity C K and O K to the Cu L peak, respectively, from EDS spectra at 5 kV.

examples shown in Figure 7. One main point from Figure 7 is that, cast 18 of 0.4Zr-0.04P at 1419 K (1146 °C) exhibited CET having a grain structure somewhat coarser than that of 0.1Ag-0.069P cast at 1423 K (1150 °C)<sup>[17]</sup> (Figure 7(b)). With the addition of Ag of 0.015 pct (Cu-0.4Zr-0.04P-0.015Ag cast at 1419 K (1146 °C) (Figure 8), no further grain refinement was observed.

P-free cast 1 of 0.4B showed CET (Figure 5), whereas cast 15 of 0.4B-0.15P exhibited CET (Figure 7) having excessive equiaxed grain coarsening. On the other hand, while cast 18 of 0.4Zr-0.04P and cast 21 of 0.4Zr-0.04P-0.015Ag gave CET (Figures 7 and 8, respectively); P-free cast 11 of 0.4Zr exhibited a mixture of large columnar grain structure / some equiaxed grains, cast 19 of 0.4Zr-0.15P and cast 20 of 0.4Zr-0.015Ag had a columnar grain structure (Figure 8). Thereby, the reason for variation in grain structure is more likely to be associated with the ease of nucleation<sup>[21]</sup> rather than the effect of B and Zr additions of 0.4 pct. Qualitative SEM-EDS analysis of particles was therefore carried out to identify particles in B- and Zr-treated casts.

#### D. Qualitative SEM-EDS Analysis of Particles in the B- and Zr-Treated Casts

##### 1. B-treated casts 1 and 15

The B-treated castings contained a large number of irregular B-rich particles which were present either as both individual, single-phase particles or as part of multiphase particles, as identified by BSE images and EDS, Figures 9 and 10. The numbers in Figure 9 represent normalized C and O peaks from EDS spectra and the ratio of peak intensities P K to B K as described earlier. The P-treated cast 15 of 0.4B-0.15P exhibited greater total amounts of particles as was observed by optical microscopy. Among the B-treated casts studied, B-rich multiphase particles found in cast 1 of 0.4B consisted of mixtures of particles richer in C and generally richer in O than the matrix (Figure 9). B- and C-containing particles arising from B-containing melt in contact with carbon, whereas, B- and O-containing particles arising from deoxidation reactions involving boron. For the P-treated cast 15 of 0.4B-0.15P (Figure 10), the core in multiphase particles being P-depleted and more C-rich compared to the outer region. While in general, the EDS results are likely to include a contribution from the surrounding matrix for the size of particles in this study, there were a number of exceptions, as shown in the EDS spectra at point 2 (inset 1), where the Cu L line intensities were below the background levels when operating at 5 kV. From point 2 (inset 1), the B to C atomic ratio was calculated to be 4.12, and those for other particles in the same cast 15 of 0.4B-0.15P were 5.96, 6.15, and 6.39, which roughly correspond to the stoichiometry of  $B_4C$ . The occurrence of these multiphase particles is consistent with the formation of  $B_4C$  in the melt, followed by  $B_xP_y$  in the melt or in the solid state depending on overall B and P levels; solid-state formation would be expected to give much finer particles. Quantification of stoichiometry of

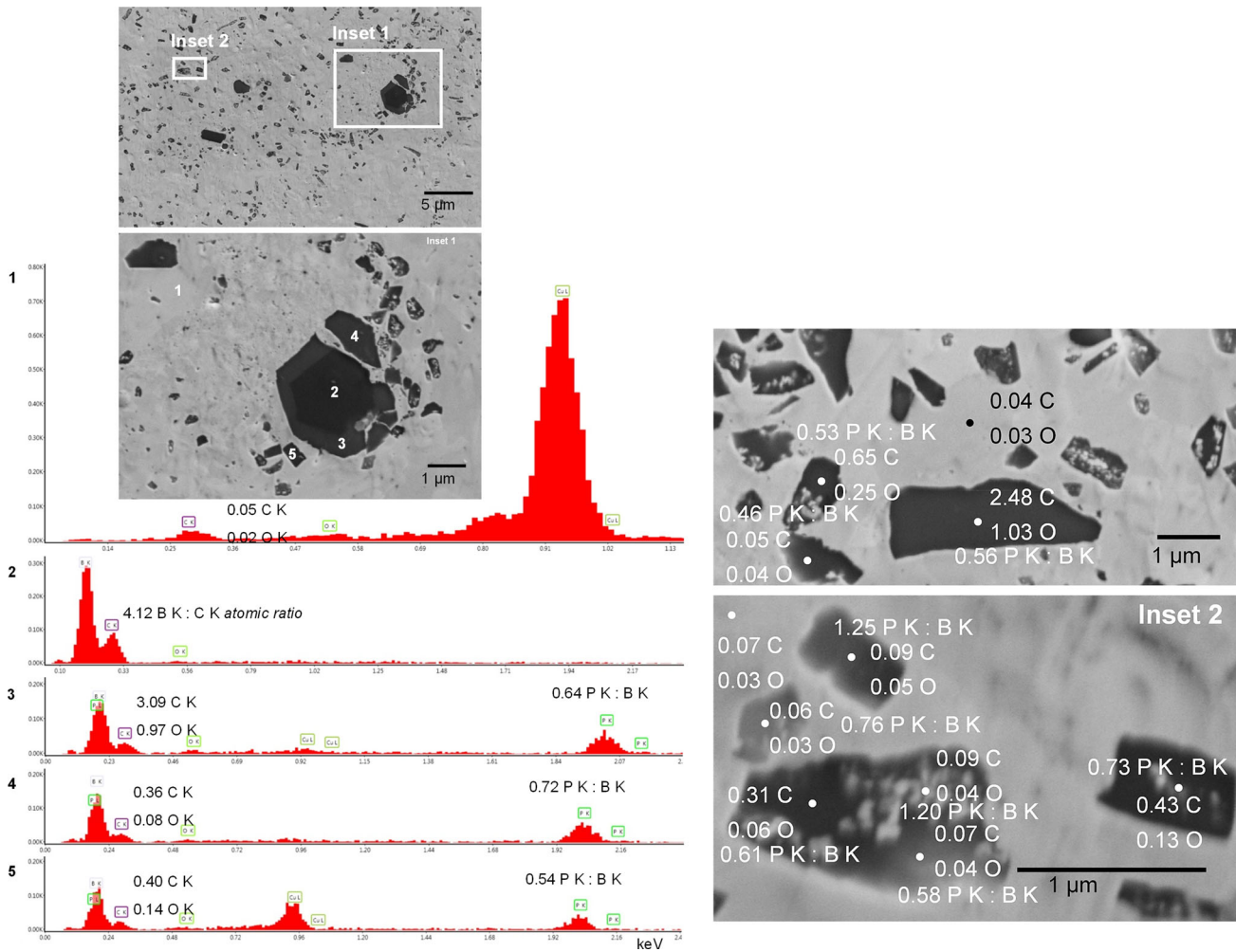


Fig. 10—SE micrographs and EDS spectra of B- and P-containing particles from cast 15 of 0.4B-0.15P. C K and O K peaks have been normalized to the Cu L peak at 5 kV. Qualitative assessment of the P and B contents were determined as the ratio of peak intensities P K to B K operating at 5 kV. The intensity axes have been kept at the same scale as a guide to the eye to allow comparison among EDS spectra.

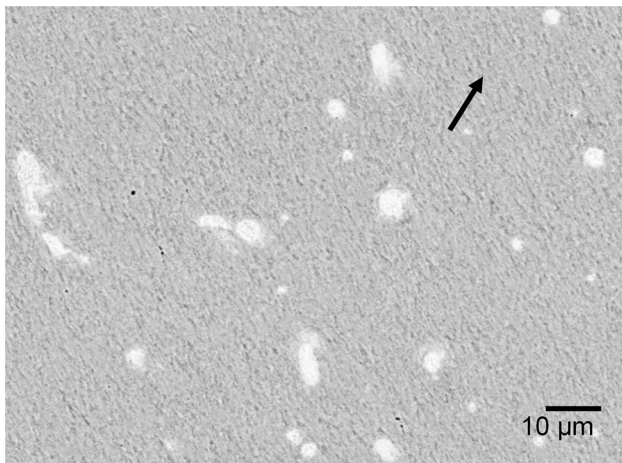


Fig. 11—SEM-BSE micrograph of Zr-containing particles from cast 11 of 0.4Zr. Grain boundary (arrowed).

$B_xP_y$  ( $B_{13}P_2$ ,  $B_6P$ , and  $BP$ ,<sup>[36]</sup> as cited in Reference 37) was made more difficult due to the possible formation of boron carbide and boron oxide particles.

$B_4C$  phase can act as an effective nucleating substrate in Cu-Al alloys.<sup>[24]</sup> In the P-free cast 1 of 0.4B (CET),  $B_4C$  particles could have potentially acted as nucleating substrates, and grain growth could have been restricted by constitutional undercooling during solidification and subsequent Zener pinning of grain boundaries (Figure 9). However, in the P-treated cast 15 of 0.4B-0.15P (CET having excessive equiaxed grain coarsening), nucleation will depend on the probability of finding single  $B_4C$  particles. As seen in Figure 10, B-containing particles (being P-depleted) tended to be encapsulated by B-containing particles being P-rich.

## 2. Zr-treated casts 11, 18-21

Qualitative SEM-EDS analysis of particles found in Zr-treated casts are shown in Figures 11 through 13. The particle morphology changed from globular, for cast 11 of 0.4Zr (Figure 11); cast 18 of 0.4Zr-0.04P (Figure 12); cast 20 of 0.4Zr-0.015Ag; and cast 21 of 0.4Zr-0.04P-0.015Ag to hexagonal morphologies; and irregular morphologies, for cast 19 of 0.4Zr-0.15P (Figure 13). Phosphorus has a high affinity for

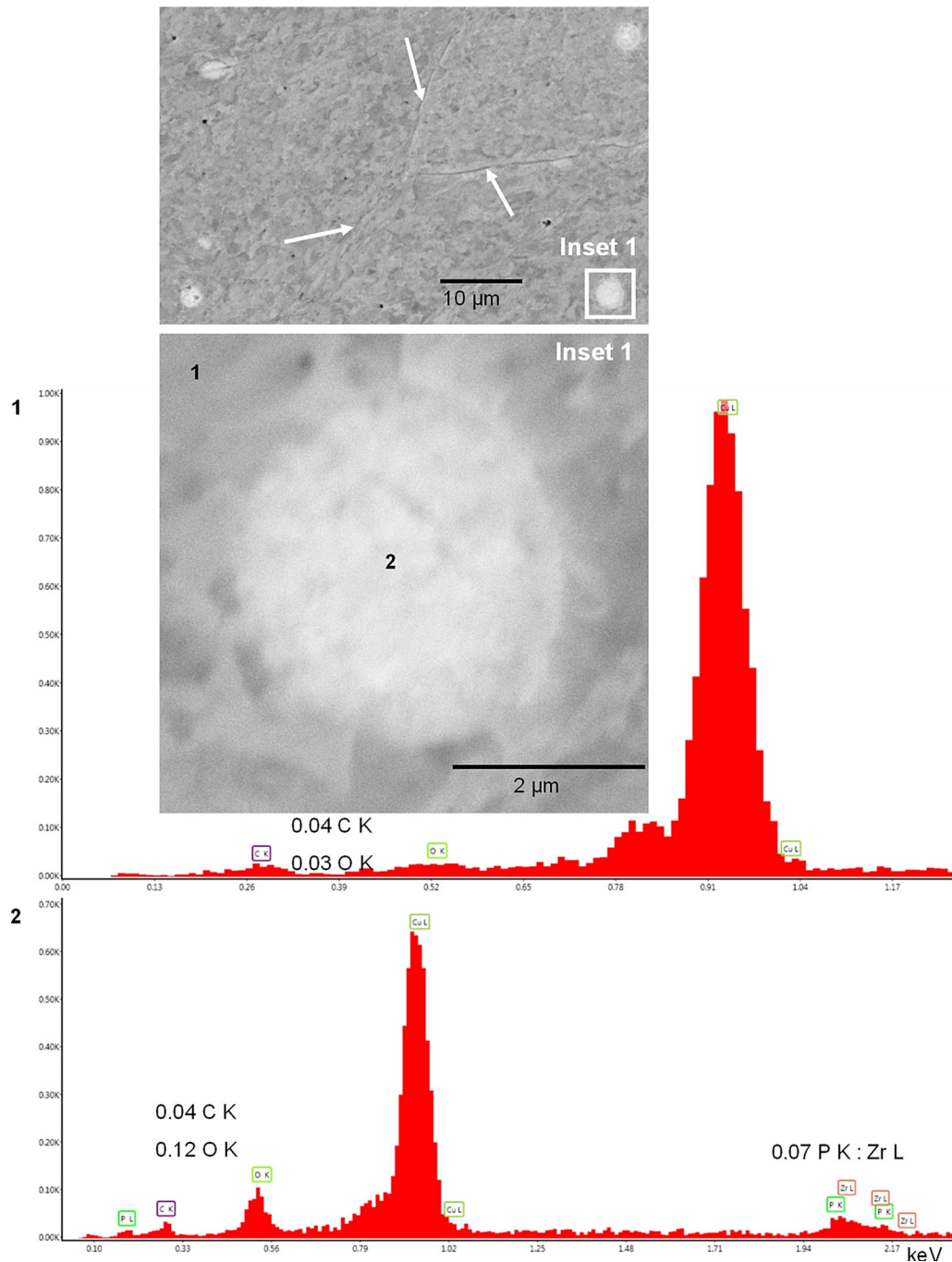


Fig. 12—SEM-BSE micrographs of typical Zr- and P-containing particles from cast 18 of 0.4Zr-0.04P. Grain boundaries (arrowed). C K and O K peaks have been normalized to the Cu L peak at 5 kV. Qualitative assessment of the P and Zr contents were determined as the ratio of peak intensities P K to Zr L operating at 25 kV.

zirconium<sup>[36]</sup> (as cited in Reference 37) (in that case at high temperatures). The numbers in Figures 12 and 13 represent, again, normalized C and O peaks from EDS spectra and the ratio of peak intensities P K to Zr L, after peak deconvolution as described earlier. Particle composition was strongly dependent on overall Zr and P levels. Zr- and P-containing particles were generally found to be Zr-rich with a P K/Zr L ratio that varied between 0.05 and 0.17, for cast 18 of 0.4Zr-0.04P and

cast 21 of 0.4Zr-0.04P-0.015Ag; and between 0.80 and 0.94, for cast 19 of 0.4Zr-0.15P. Isolated examples of hexagonal-shaped particles richer in P were also observed in cast 18 of 0.4Zr-0.04P (an example of peak intensity ratio P K/Zr L is 0.85), but in insufficient numbers to be significant. The P K/Zr L ratio varied with particle size for cast 19 of 0.4Zr-0.15P, with coarser particles generally having a lower P K/Zr L ratio (Zr-richer) (Figure 13).

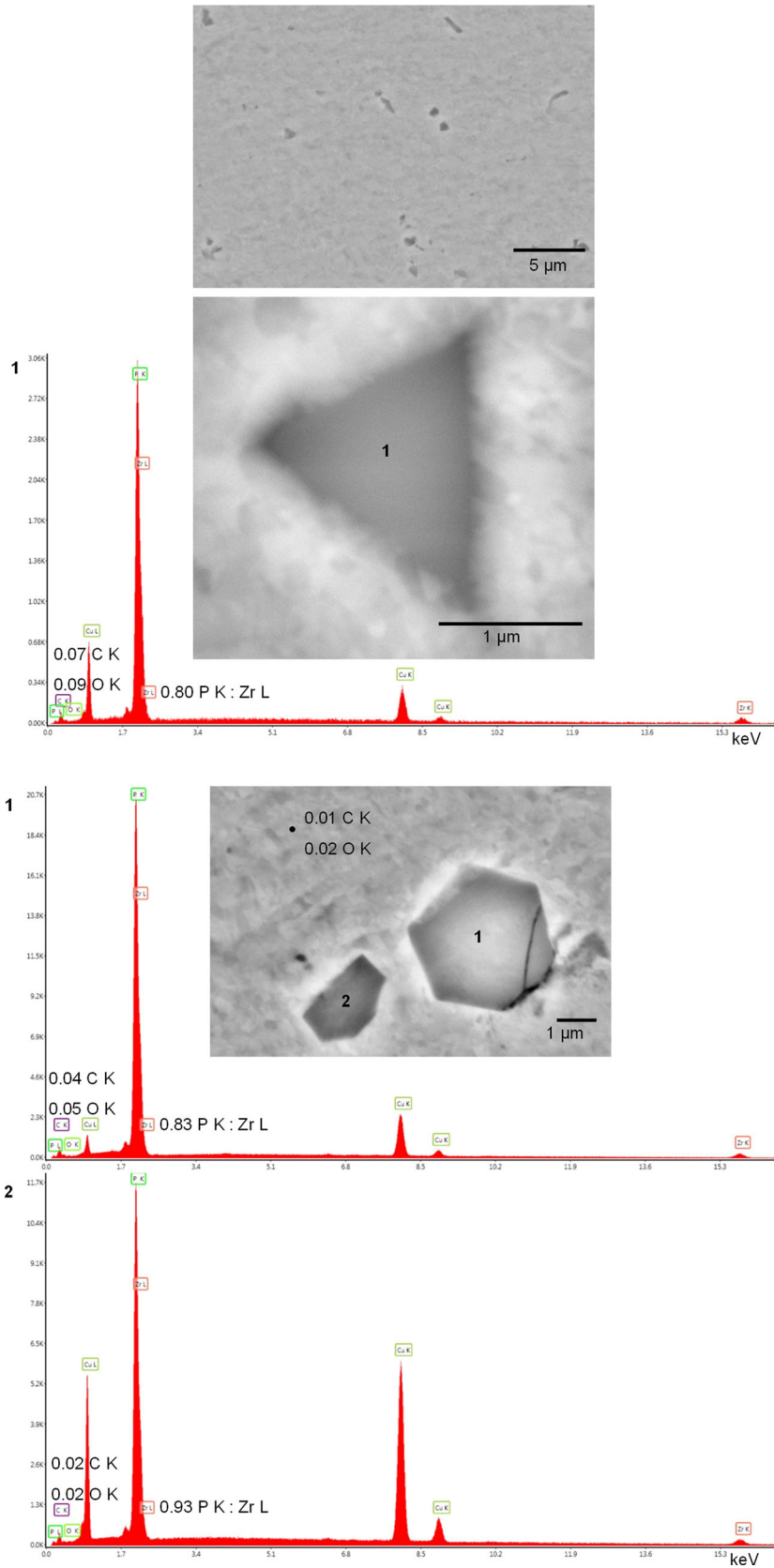


Fig. 13—SEM-BSE micrographs of Zr- and P-containing particles from cast 19 of 0.4Zr-0.15P. C K and O K peaks have been normalized to the Cu L peak at 5 kV. Qualitative assessment of the P and Zr contents was determined as the ratio of peak intensities P K to Zr K operating at 25 kV. Note the Zr K peaks.



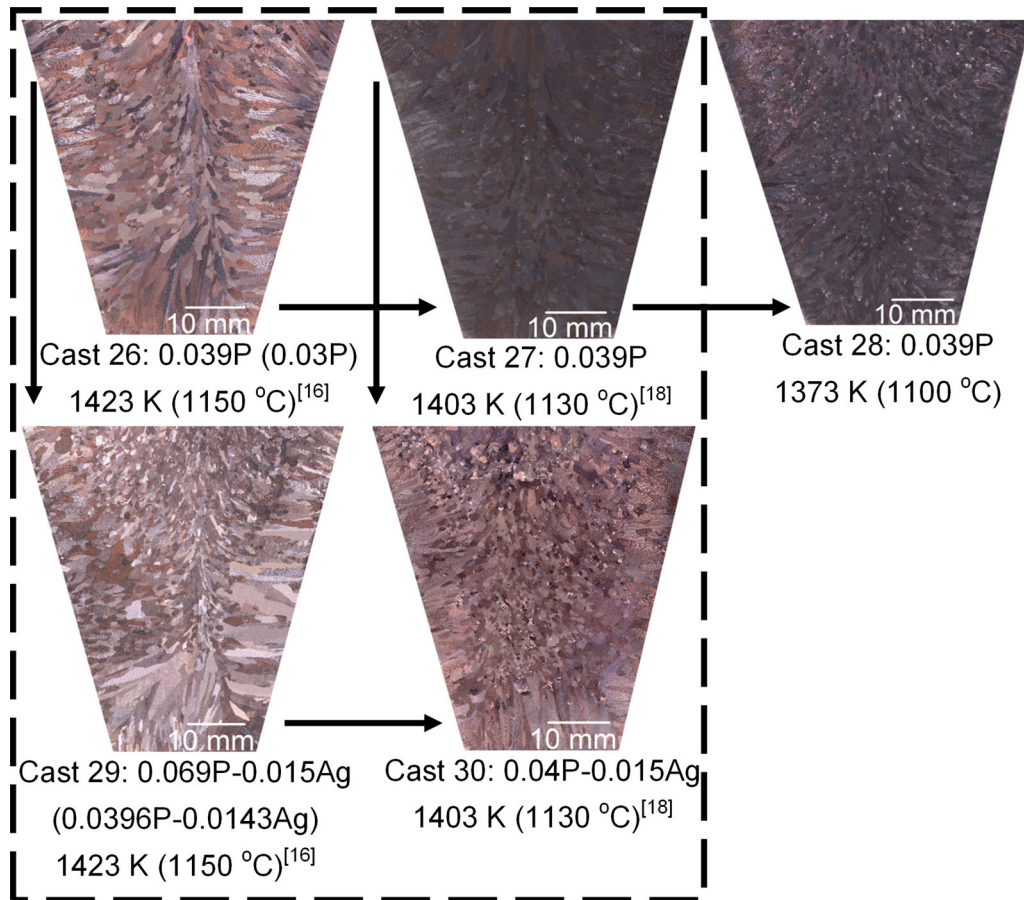


Fig. 14—Effects of casting temperature (horizontal arrows) and a microalloying addition of 150 ppm Ag (vertical arrows) on the grain structure of DHP-Cu from Table IV. Note that macrographs of DHP-Cu reference with and without microalloying with Ag and cast at 1423 K and 1403 K (1150 °C and 1130 °C) are shown within the dashed box. Casting temperatures are shown for each TP-1 sample. Macrographs from casts 26 and 29 are reprinted with permission from Ref. [16], copyright 2015, Taylor & Francis Ltd, [www.tandfonline.com](http://www.tandfonline.com). Macrographs from casts 27 and 30 are reprinted with permission from Ref. [18], copyright 2015, Tanger.

### E. P and Ag Microalloying Additions

The effects of P (0.039 and 0.069 pct) and Ag (150 ppm) on microalloying additions and casting temperatures of 1423 K (1150 °C),<sup>[16]</sup> 1403 K (1130 °C)<sup>[18]</sup> and 1373 K (1100 °C) on the macrostructure are given in Table IV and shown in Figure 14, from which it can be seen that they exhibit some different extents of degrees of CET. A greater degree of CET was obtained: (i) on decreasing the casting temperature from 1423 K (1150 °C)<sup>[16]</sup> to 1403 K (1130 °C)<sup>[18]</sup> to 1373 K (1100 °C) (horizontal arrows), for fixed addition of: 0.039 pct P (cf. casts 26–28) and of 150 ppm Ag (cf. casts 29 and 30); and (ii) with a microalloying addition of 150 ppm Ag (vertical arrows), for a given casting temperature (cf. casts 26 and 29)<sup>[16]</sup> and (cf. casts 27 and 30).<sup>[18]</sup> This behavior indicates that the microalloying addition of 150 ppm Ag to DHP-Cu was essential for grain size control at 1423 (1150 °C) and 1403 K (1130 °C).

### F. Microalloying Additions to DHP-Cu Microalloyed with Ag

The effects of the de-embrittling elements of copper—B, Mg, Ca, Zr, and Ti—in concentrations of

0.085–0.17 pct without the addition of Ag and cast at 1423 K (1150 °C)<sup>[17]</sup> and with the addition of Ag of 150 ppm and cast at 1403 K (1130 °C)<sup>[18]</sup> on the resulting macrostructure of DHP-Cu in general have been summarized in the first part of Table V (casts 31–40).

Since cast 18 of 0.4Zr-0.04P exhibited CET at 1419 K (1146 °C), an increased nominal addition of Zr to 0.15 pct was made to DHP-Cu microalloyed with Ag (cast 38) to enhance the content of Zr in the copper sample, followed by casting at 1403 K (1130 °C). The level of Zr microalloying element was, indeed, found to be high (1107 ppm) in cast 38 having CET to a lesser extent compared to that of the corresponding DHP-Cu reference cast 30 of 0.04P-0.015Ag at 1403 K (1130 °C) (shown in the dashed box in Figure 14).

On the other hand, within the Mn + P + Ag, In + P + Ag, Fe + P + Ag, and Zn + P + Ag casts studied (see Table V and Figure 15), the grain structures varied from large columnar for casts 43 and 50 to CETs somewhat coarser than those of the corresponding DHP-Cu references for casts 44, 45, 48, 49, and 51, and to CET for cast 46. This is indicative of a loss of effect of constitutional undercooling on grain growth inhibition and could result from the simultaneous

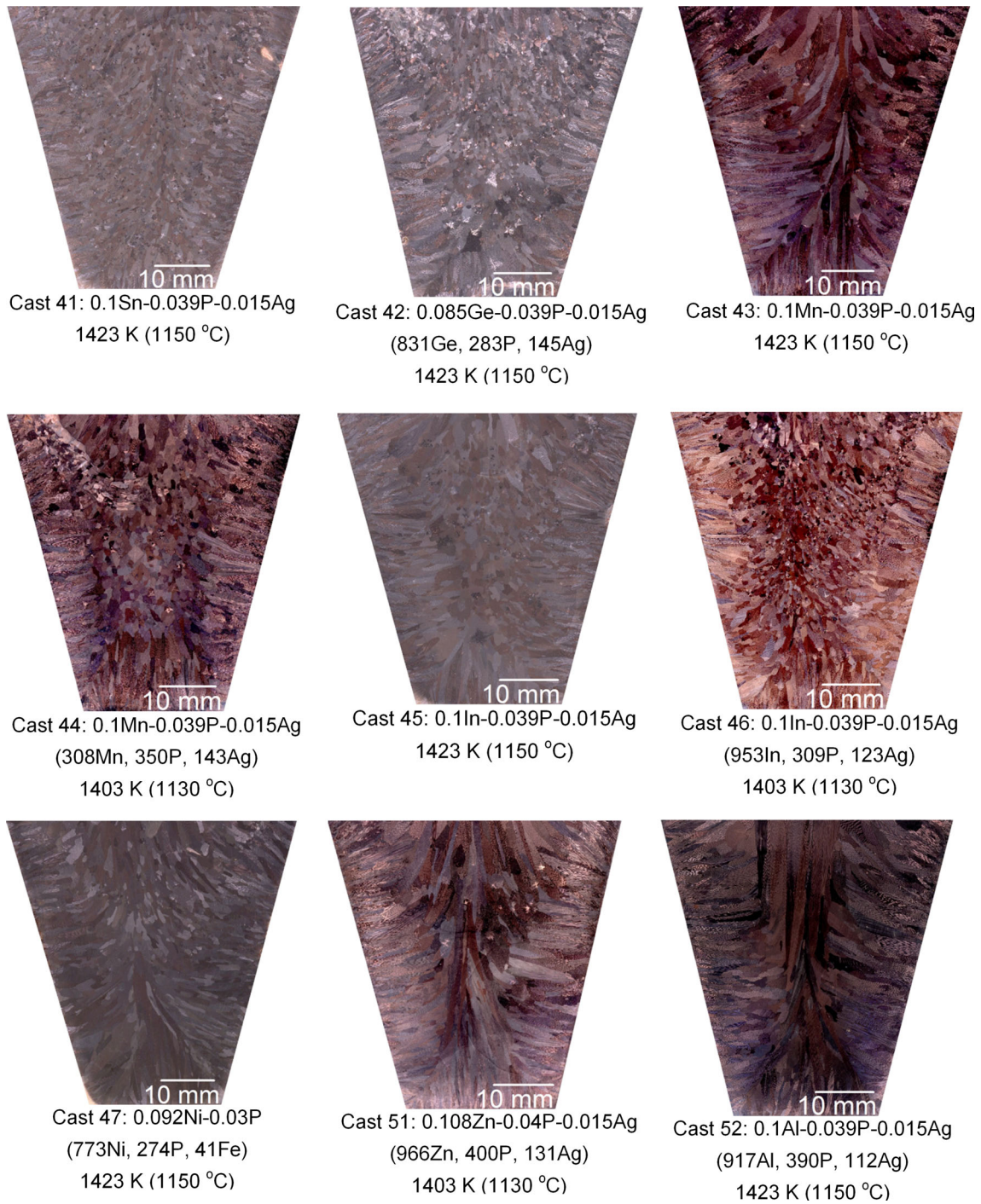


Fig. 15—Macrographs of DHP-Cu from Table V cast at 1423 K and 1403 K (1150 °C and 1130 °C).

**Table IV. DHP-Cu Reference With and Without Microalloying with Ag**

Cast		Casting T [K (°C)]	Nominal Compositions (Wt Pct)	ICP-OES Trace Analysis (Wt ppm)	Macrostructure
26	P <sup>[16]</sup>	1423 (1150)	0.039P	300P	CET to a lesser extent
27	P <sup>[18]</sup>	1403 (1130)	0.039P		CET to a lesser extent
28	P	1373 (1100)	0.039P		CET
29	P + Ag <sup>[16]</sup>	1423 (1150)	0.069P, 0.015Ag	396P, 143Ag	CET to a lesser extent
30	P + Ag <sup>[18]</sup>	1403 (1130)	0.039P, 0.015Ag		CET

**Table V. Nominal and Chemical Compositions of Investigated Additions to DHP-Cu and Macrostructure**

Cast	Oxides	Density (kg/m <sup>3</sup> ) <sup>[65]</sup> × 10 <sup>-3</sup>	Melting Point <sup>[65]</sup> [K (°C)]	Casting T [K (°C)]	Nominal Compositions (Wt Pct)	ICP-OES Trace Analysis (Wt ppm)	Master Alloys/ Materials (Wt Pct)	Macrostructure
31	B + P <sup>[17]</sup> B <sub>2</sub> O <sub>3</sub>	2.55	723 (450)	1423 (1150)	0.170B, 0.0690P	262B, 260P		CET excessive equiaxed grain coarsening
32	B + P + Ag <sup>[18]</sup> MgO	3.6	3098 (2825)	1403 (1130)	0.1B, 0.039P, 0.015Ag	754Mg, 218P	Ag (99.9)	CET excessive equiaxed grain coarsening large columnar
33	Mg + P <sup>[17]</sup>	3.6	3098 (2825)	1423 (1150)	0.085Mg, 0.03P	754Mg, 218P		CET excessive equiaxed grain coarsening
34	Mg + P + Ag <sup>[18]</sup>	3.6	3098 (2825)	1403 (1130)	0.1Mg, 0.039P, 0.015Ag	754Mg, 218P		CET excessive equiaxed grain coarsening
35	Ca + P <sup>[17]</sup>	3.34	3171 (2898)	1423 (1150)	0.085Ca, 0.03P	448Ca, 264P		large columnar
36	Ca + P + Ag <sup>[18]</sup>	3.34	3171 (2898)	1403 (1130)	0.1Ca, 0.039P, 0.015Ag	547Ca, 390P, 145Ag		CET to a lesser extent
37	Zr + P <sup>[17]</sup>	5.68	2982 (2709)	1423 (1150)	0.085Zr, 0.03P	166Zr, 250P		large columnar
38	Zr + P + Ag	5.68	2982 (2709)	1403 (1130)	0.15Zr, 0.04P, 0.015Ag	1107Zr*, 360P, 96Ag		CET to a lesser extent
39	Ti + P <sup>[17]</sup>	4.95	2023 (1750)	1423 (1150)	0.085Ti, 0.039P	16Ti, 305P		CET to a lesser extent
40	Ti + P + Ag	4.95	2023 (1750)	1423 (1150)	0.116Ti, 0.04P, 0.0203Ag*	955Ti, 399P, 184Ag*		CET to a lesser extent
41	Sn + P + Ag	6.45	1353 (1080), 1903 (1630)	1423 (1150)	0.15Sn, 0.039P, 0.015Ag			CET
42	Ge + P + Ag	4.25	1388 (1115)	1423 (1150)	0.085Ge, 0.039P, 0.015Ag	831Ge, 283P, 145Ag	Ge-[0.1-0.5] Ga (99.999 metal basis)	CET
43	Mn + P + Ag	5.37	2112 (1839), 1353 (1080)	1423 (1150)	0.1Mn, 0.039P, 0.015Ag	308Mn, 350P, 143Ag	99.7min.Mn- 0.04max.C-0.05max.S- 0.005max.P- 0.205max.Fe + Si + Se	large columnar
44	Mn <sub>2</sub> O <sub>3</sub>	5.0	1353 (1080)	1403 (1130)	0.1Mn, 0.039P, 0.015Ag			CET to a lesser extent
45	In + P + Ag	7.18	2185 (1912)	1423 (1150)	0.1In, 0.039P, 0.015Ag			CET to a lesser extent
46	In <sub>2</sub> O <sub>3</sub>	7.18	2185 (1912)	1403 (1130)	0.1In, 0.039P, 0.015Ag	953In, 309P, 123Ag	In (99.99)	CET
47	Ni + P	6.72	2228 (1955)	1423 (1150)	0.092Ni, 0.03P	773Ni, 274P, 41Fe, 20Mn	Cu-31Ni-1Mn-0.7Fe	columnar
48	Fe + P + Ag	5.25	1838 (1565), 1870 (1597)	1423 (1150)	0.721Fe, 0.039P, 0.015Ag	643Fe, 300P, 138Ag	Cu-10.2Fe-0.08Pb- 0.01Sn-0.02Mn- 0.02Zn-0.005Al- 0.005Si	CET to a lesser extent
49	Fe <sub>2</sub> O <sub>3</sub> , Fe <sub>3</sub> O <sub>4</sub>	5.25	1838 (1565), 1870 (1597)	1423 (1150)	0.721Fe, 0.039P, 0.015Ag	643Fe, 300P, 138Ag		CET to a lesser extent
50	Zn + P + Ag	5.6	2247 (1974)	1423 (1150)	0.1Zn, 0.039P, 0.015Ag			large columnar
51	ZnO	5.6	2247 (1974)	1403 (1130)	0.108Zn, 0.04P, 0.015Ag	966Zn, 400P, 131Ag	Zn (99.9)	CET to a lesser extent
52	Al + P + Ag	3.97	2326 (2053)	1423 (1150)	0.1Al, 0.039P, 0.015Ag	917Al, 390P, 112Ag	Al (99.99)	large columnar

\*Marginally outside the DHP-Cu specification limit to enhance their effect on grain structure.

CET to a lesser extent compared to that of the corresponding DHP-Cu reference casts from Table IV (shown in the dashed box in Figure 14).

Casts 31, 33, 35, 37, and 39 are reprinted with permission from Ref. 17, copyright 2015, Taylor & Francis Ltd, [www.tandfonline.com](http://www.tandfonline.com).

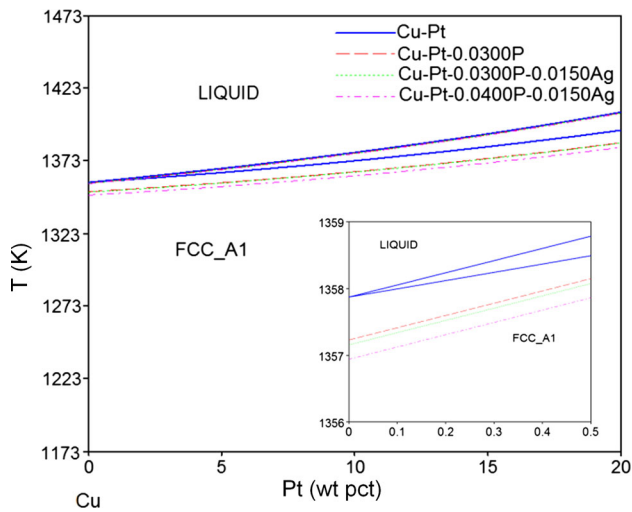


Fig. 16—Development of the Cu-rich region of the equilibrium phase diagram for the Cu-Pt alloy modified with 300 ppm P, 400 ppm P, and 150 ppm Ag (for interpretation of the references to color in this figure, the reader is referred to the web version of this article).

reaction of P in the liquid melt to form phosphides with different ratios of phosphorus and metal atoms, *i.e.*, metal-rich phosphides, monophosphides, and phosphorus-rich phosphides, examples of which are  $Zr_3P$ ,  $Zr_2P$ ,  $Zr_7P_4$ ,  $Zr_{14}P_9$ ,  $ZrP$ ,  $ZrP_2$ ,  $Mn_3P$ ,  $Mn_2P$ ,  $MnP$ ,  $MnP_4$ ,  $InP$ ,  $InP_3$ ,  $Fe_3P$ ,  $Fe_2P$ ,  $FeP$ ,  $FeP_2$ ,  $FeP_4$ ,  $Zn_3P_2$ ,  $ZnP$ , and  $ZnP_2$  (as cited in Reference 37).<sup>[36]</sup> Hence, individual Zr, Mn, In, Fe, and Zn microalloying additions in concentrations of  $\sim 0.1$  pct to DHP-Cu are no longer needed, for the casting conditions studied here. This makes the microalloying with the addition of Ag of 0.015 pct to DHP-Cu necessary for grain size control under TP-1 casting conditions, as presented elsewhere.<sup>[18]</sup> On increasing the level of Zr in the base composition from 0.1 to 0.4 pct, having 0.04 pct P with and without microalloying with Ag, the effect of Zr on restricting grain growth was seen for cast 18 of 0.4Zr-0.04P and cast 21 of 0.4Zr-0.04P-0.015Ag, where Zr-rich and low P-containing particles could have acted as potent nucleation sites.

Note from Figure 15 that the effect of the combined addition of Al + Ag + P on the grain structure of DHP-Cu epitomizes an unrestricted type of columnar grain growth under high thermal gradient (from liquid to solid). This behavior has been previously reported for the binary Cu-Al system.<sup>[1]</sup> The freezing range at 0.1 pct of solute addition (Table I) for the binary Cu-Al alloy (Figure A1(o)) is small (0.02 K) and similar to that (0.16 K) for the binary Cu-Pt alloy (Figure 16), although a strong grain-refining effect in copper has been observed in the latter case for Pt additions of 0.25 and 0.5 pct.<sup>[1]</sup> This was suggested to be indicative of atomic interactions independently of the type of alloy formed.<sup>[1]</sup>

## V. CONCLUSIONS

This study has examined the topic of grain refinement of copper accompanied by a critical appraisal of grain refinement of microalloyed DHP-Cu and cast under TP-1 casting conditions. The main conclusions are as follows.

1. Some divergences existed in terms of the growth restriction factor  $Q$  framework. This evidence is gleaned from the analysis of available data on grain size measurements of copper with individual additions of 0.05, 0.1, and 0.5 pct of Mo, In, Sn, Bi, Sb, Pb, and Se, cast under a protective atmosphere of pure Ar and water quenching.
2. The columnar-to-equiaxed transition (CET) was observed in copper with an individual addition of 0.4B and with combined additions of 0.4Zr-0.04P; 0.4Zr-0.04P-0.015Ag; and 0.1Ag-0.069P (in wt pct).
3. Irregular B-containing particles (being P-depleted) were present in the 0.4B cast and could have acted as potent nucleation sites in copper. With the combined addition of 0.4 pct B and 0.15 pct P into copper, B-containing particles (being P-depleted) tended to be encapsulated by B-containing particles being P-rich particles, causing poisoning and excessive coarsening of equiaxed grains.
4. On increasing the level of P in the base composition of Zr-treated casts, the particle morphology changed from globular for the 0.4Zr; 0.4Zr-0.04P; 0.4Zr-0.015Ag, and 0.4Zr-0.04P-0.015Ag casts to hexagonal, and irregular morphologies for the 0.4Zr-0.15P cast, and the Zr-rich and P-containing particles become richer in P. Zr-rich and low P-containing particles in 0.4Zr-0.04P and 0.4Zr-0.04P-0.015Ag casts could have acted as potent nucleation sites in copper.
5. In comparison with the corresponding DHP-Cu reference cast at 1423 K and 1403 K (1150 °C and 1130 °C), no further grain-refining action was observed due to microalloying additions of B, Mg, Ca, Zr, Ti, Mn, In, Fe, and Zn ( $\sim 0.1$  pct) with respect to DHP-Cu microalloyed with Ag, and therefore are no longer relevant for the casting conditions studied. The high P reactivity to form metal, nonmetal, and transition metal phosphides could account for the loss of solute constitutional undercooling effect ( $\sim 0.1$  pct solute) on grain growth inhibition.
6. The critical microalloying element for grain size control in deoxidized copper and in particular DHP-Cu is Ag. An addition of 0.1 pct Ag to deoxidized copper gave the strongest grain-refining action at a casting temperature of 1423 K (1150 °C) achieving CET. An addition of 150 ppm Ag to DHP-Cu gave the strongest grain-refining action at both casting temperatures of 1423 K and 1403 K (1150 °C and 1130 °C) achieving CET.

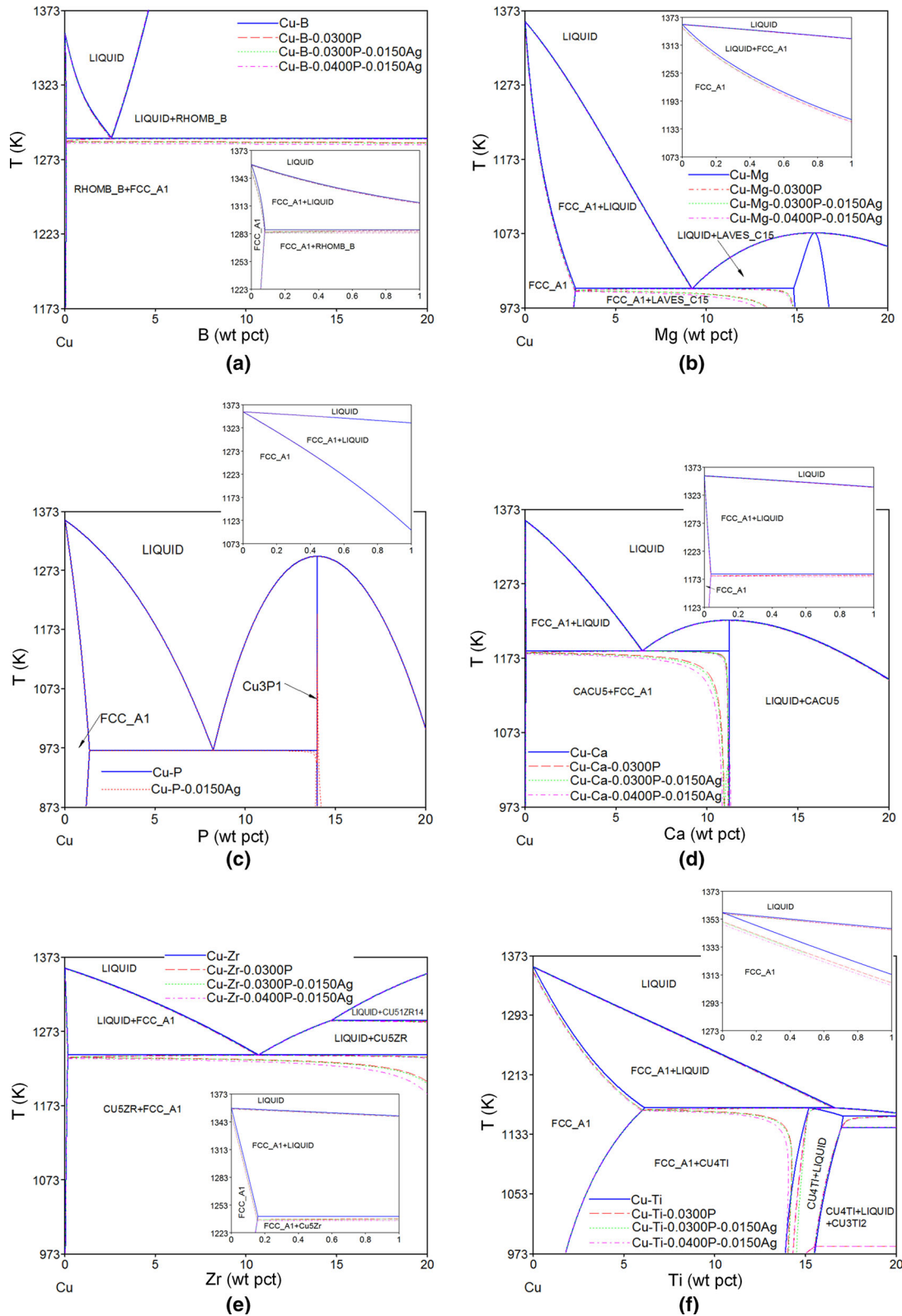


Fig. A1—Development of the Cu-rich regions of the equilibrium phase diagrams for the investigated alloy systems containing (a) B, (b) Mg, (c) P, (d) Ca, (e) Zr, (f) Ti, (g) Sn, (h) Ge, (i) Mn, (j) In, (k) Ni, (l) Ag, (m) Fe, (n) Zn, (o) Al, and (p) Cu-Mo binary system at the corresponding fixed contents of 300 ppm P, 400 ppm P, and 150 ppm Ag and their magnified regions (small insets). Note 400 ppm P and 150 ppm Ag are upper bound values of the DHP-Cu specification limits (for interpretation of the references to color in this figure, the reader is referred to the web version of this article). Cu-P binary, Cu-X binary, and Cu-X-300P ternary systems (where  $X = B, Mg, Ca, Zr, Ti, \text{ and } Ag$ ) are reprinted with permission from Ref. [17], copyright 2015, Taylor & Francis Ltd, [www.tandfonline.com](http://www.tandfonline.com).

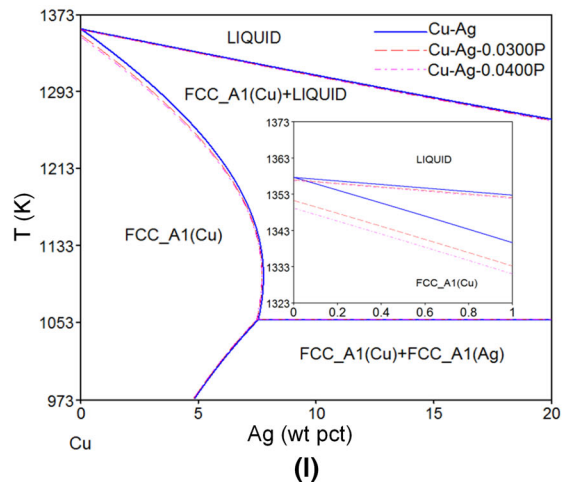
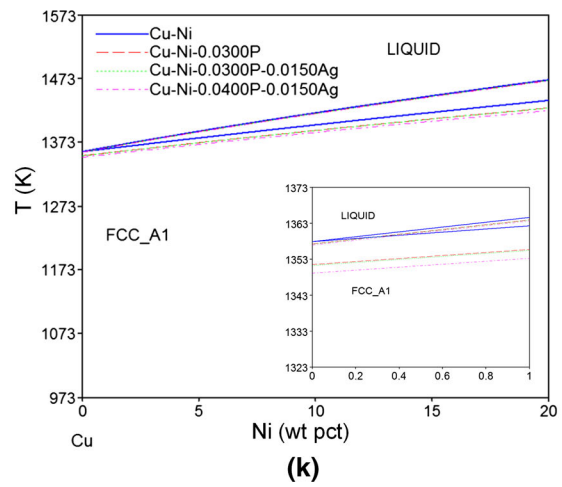
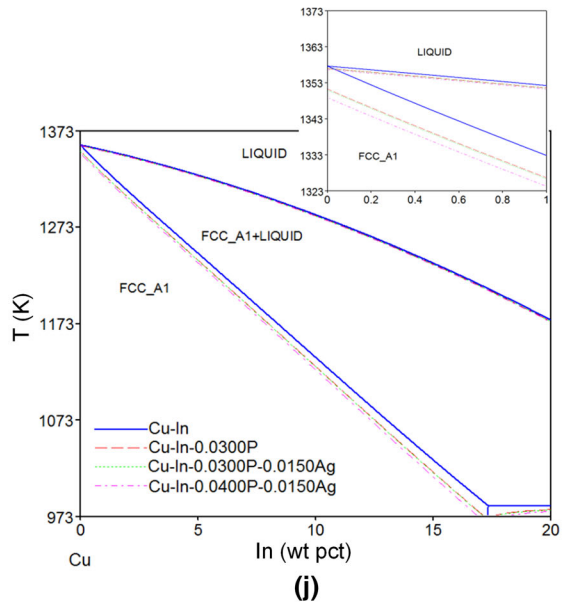
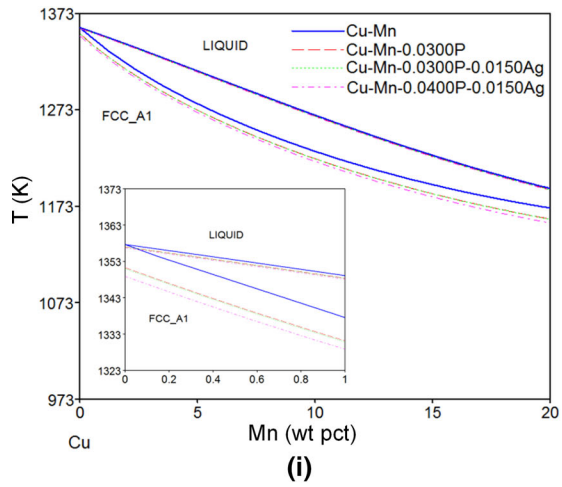
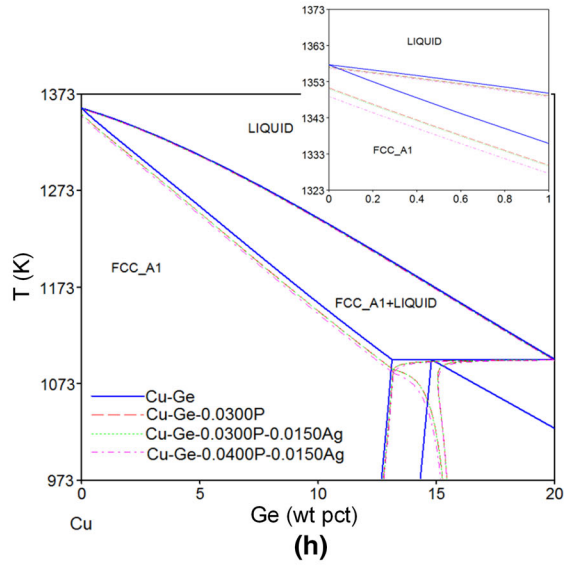
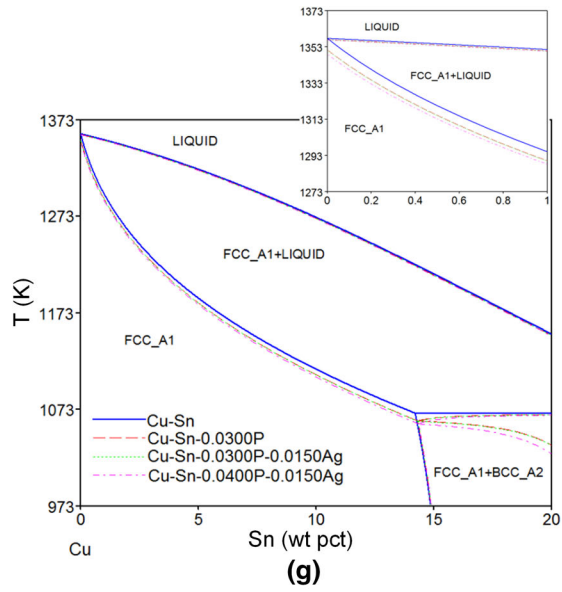


Fig. A1—continued.

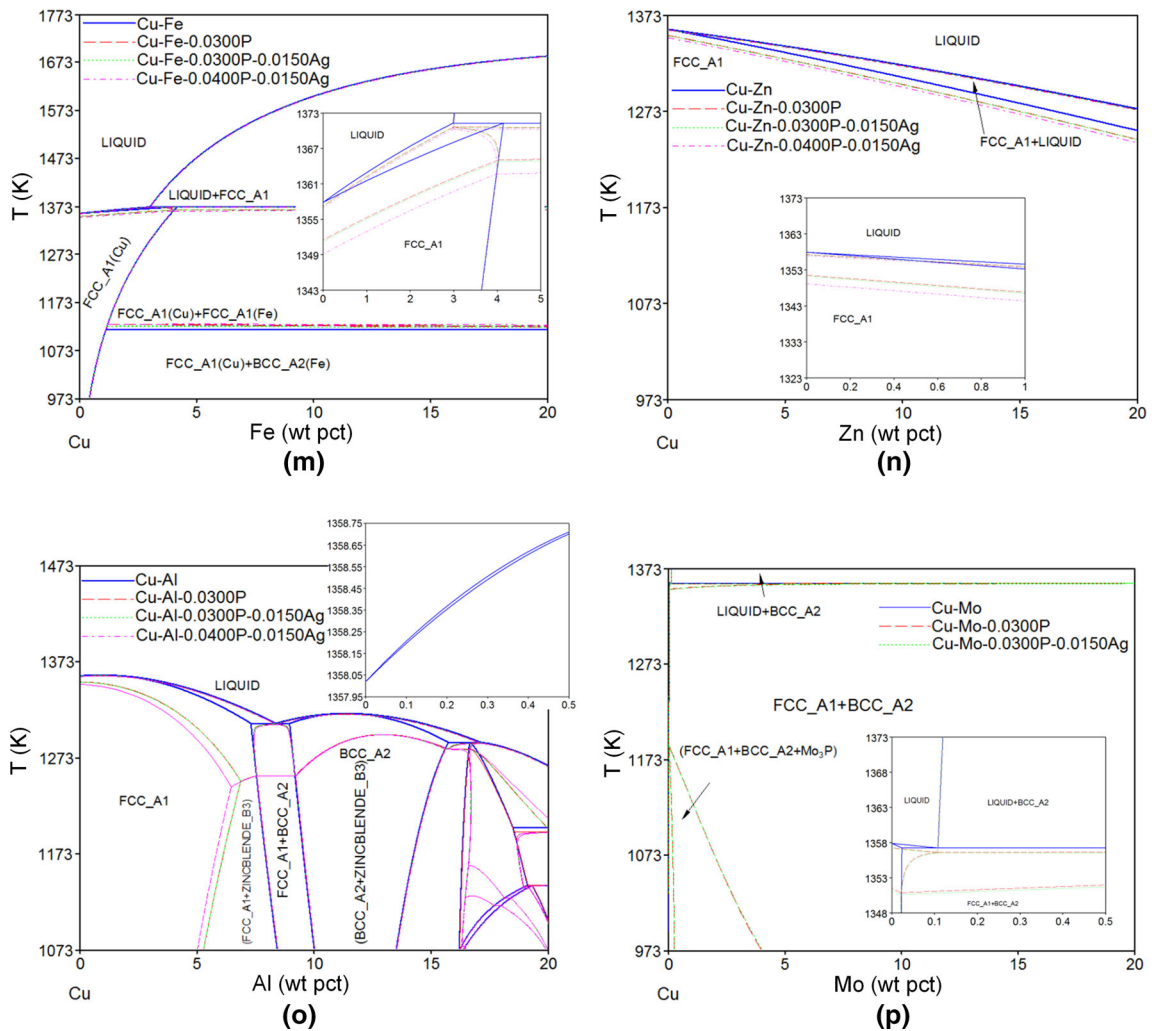


Fig. A1—continued.

## ACKNOWLEDGMENTS

The financial support from the EPSRC and the supply of Cu-CATH-1 by Rautomead Ltd. are gratefully acknowledged. Thanks are also due to the Experimental Techniques Centre (ETC) for the provision of the FEG-SEM research facility at Brunel University London and their assistance in this work.

## OPEN ACCESS

This article is distributed under the terms of the Creative Commons Attribution 4.0 International License (<http://creativecommons.org/licenses/by/4.0/>), which permits unrestricted use, distribution, and reproduction in any medium, provided you give appropriate credit to the original author(s) and the source, provide a link to the Creative Commons license, and indicate if changes were made.

## APPENDIX: THERMODYNAMIC ANALYSIS

The Cu-rich region of the corresponding equilibrium phase diagrams were generally predicted for binary

Cu- $X$  systems (where  $X = B, Mg, P, Ca, Zr, Ti, Sn, Ge, Mn, In, Ni, Ag, Fe, Zn, Al, Mo, etc.$  (see Table I)) and the corresponding ternary Cu- $X$ -0.03P, and quaternary Cu- $X$ -0.03P-0.015Ag and Cu- $X$ -0.04P-0.0150Ag systems, for additions of up to 20 pct and having fixed P contents of 300 ppm and 400 ppm and a fixed Ag content of 150 ppm. The latter two are upper bound values of the DHP-Cu specification limits. The predictions were made using the software package Pandat (version 8.0). The binary Cu-Sr phase diagram was predicted using Thermo-Calc software. Other binary phase diagrams were found in the literature: Cu-O,<sup>[42]</sup> Cu-S,<sup>[24,42]</sup> Cu-Te,<sup>[43]</sup> and Cu-Se.<sup>[24]</sup>

## REFERENCES

1. L. Northcott: *J. Inst. Met.*, 1938, vol. 62, pp. 101–36.
2. G.C. Gould, G.W. Form, and J.F. Wallace: *Trans. AFS*, 1960, vol. 68, pp. 258–67.
3. O.L. Bustos and W. Reif: *Metall.*, 1993, vol. 47 (11), pp. 1005–14.
4. O.L. Bustos and W. Reif: *Metall.*, 1994, vol. 48 (2), pp. 123–27.
5. O.L. Bustos and W. Reif: *Metall.*, 1994, vol. 48 (7), pp. 538–48.
6. W. Reif: *Metall.*, 1998, vol. 52 (3), pp. 120–30.

7. Copper Development Association: Publication No. 120, Hertfordshire, UK, April 1998, Revised and reprinted December 2004. <http://copperalliance.org.uk/docs/librariesprovider5/resources/pub-120-copper-and-copper-alloys.pdf>. Accessed 3 June 2016.
8. New UPGCAST® Developments Target Copper Tube Production and Environmental Benefits. *Technology News International*. 2010. vol. 99. pp. 28–29.
9. E.R. Bagherian, C. Bell, M. Cooper, Y. Fan, B. Frame, and A. Abdolvand: Influence of Casting Speed on the Structure and Mechanical Properties of Continuous Cast DHP Copper Tube. In *METAL 2014: 23rd International Conference on Metallurgy and Materials*. Brno, Czech Republic: EU. Ostrava: TANGER, 2014, pp. 1163–68.
10. C.-A. Gandin, J.-L. Desbiolles, M. Rappaz, M. Swierkosz, and P. Thévoz. 3D Modelling of Grain Structure Formation during Solidification. <http://dit-archives.epfl.ch/SCR96/scr-96.html>. Accessed 15 September 2015.
11. R.U. Ayres, L.W. Ayres, and I. Råde: Report No. 24, Mining, Minerals and Sustainable Development MMSD, France, January 2002. <http://pubs.iied.org/pdfs/G00740.pdf>. Accessed 5 June 2016.
12. Standard test procedure for aluminum alloy grain refiners: TP-1. The Aluminum Association, Washington DC, 1987.
13. V Laporte and A Mortensen: *Int. Mater. Rev.*, 2009, vol. 54 (2), pp. 94–116.
14. L. Felberbaum: Microstructure and Embrittlement of Leaded Copper Alloys. Ph.D. Thesis, École Polytechnique Fédérale de Lausanne EPFL, Switzerland, 2005, pp. 29, 33–34. [http://commission-recherche.epfl.ch/files/content/sites/commissionrecherche/files/Prix%20de%20recherche%2006/Felberbaum\\_Laurent.pdf](http://commission-recherche.epfl.ch/files/content/sites/commissionrecherche/files/Prix%20de%20recherche%2006/Felberbaum_Laurent.pdf). Accessed 12 Jan 2015.
15. T. Freiling: Bismuth Induced Embrittlement of a Copper Substrate. M.Sc. Thesis, University of Missouri, United States, 2012, p. 8–9.
16. M.J. Balart, J.B. Patel, and Z. Fan: *Int. J. Cast Met. Res.*, 2015, vol. 28 (4), pp. 242–47.
17. M.J. Balart, J.B. Patel, F. Gao, and Z. Fan: *Int. J. Cast Met. Res.*, 2015, vol. 28 (4), pp. 248–56.
18. M.J. Balart, J.B. Patel, F. Gao, and Z. Fan: Effects of Casting Temperature and Microalloying Elements on the Grain Structure of DHP Copper. *24th Int. Conf. on Metallurgy and Materials* (Brno; Czech Republic; 3–5 June 2015), pp. 1376–81.
19. W. Kurz, C. Bezençon, and M. Gäumann: *Sci. Technol. Adv. Mater.*, 2001, vol. 2, pp. 185–91.
20. J.D. Hunt: *Mater. Sci. Eng.*, 1984, vol. 65, pp. 75–83.
21. Z. Fan: *Metall. Mater. Trans. A*, 2013, vol. 44A, pp. 1409–18.
22. H. Men and Z. Fan: *Acta Mater.*, 2011, vol. 59, pp. 2704–12.
23. M.E. Watkins: A Comparison of Physical Properties of OF Copper and ETP Copper After Holding at Temperatures That Simulate High Voltage Transformer Use for up to One Year. *IEEE Transmission and Distribution Conference and Exposition (T&D)* (Orlando, FL; 7–10 May 2012). [http://ieeexplore.ieee.org/xpls/abs\\_all.jsp?arnumber=6281588](http://ieeexplore.ieee.org/xpls/abs_all.jsp?arnumber=6281588). Accessed 12 Jan 2015.
24. J.R. Davis (Editor): *Copper and Copper Alloys, ASM Speciality Handbook*. 2nd ed., Asm International, Materials Park, OH, 2008, pp. 7, 171–94, 360–61, 376.
25. K.F. Kobayashi and P.H. Shingu: *J. Mater. Sci.*, 1988, vol. 23, pp. 2157–66.
26. S. Walder and P.L. Ryder: *Acta Metall. Mater.*, 1995, vol. 43 (11), pp. 4007–13.
27. D.H. StJohn, M. Qian, M.A. Easton, P. Cao, and Z. Hildebrand: *Metall. Mater. Trans. A*, 2005, vol. 36A, pp. 1669–79.
28. Y.C. Lee, A.K. Dahle, and D.H. StJohn: *Metall. Mater. Trans. A*, 2013, vol. 31A, pp. 2895–2906.
29. M.A. Easton and D.H. StJohn: *Metall. Mater. Trans. A*, 2005, vol. 36A, pp. 1911–20.
30. A. Kozlov and R. Schmid-Fetzer: Growth Restriction Factor in Al-Si-Mg-Cu Alloys. *3rd Int. Conf. on Advances in Solidification Processes, IOP Conf. Series: Materials Science and Engineering*, 2011, vol. 27.
31. A. López and E.J. Mittemeijer: *Scripta Mater.*, 2004, vol. 51, pp. 1–5.
32. A. Mirak, C.J. Davidson, and J.A. Taylor: *Corros. Sci.*, 2010, vol. 52, pp. 1992–2000.
33. H.J.T. Ellingham: *J. Soc. Chem. Ind.*, 1944, vol. 63, pp. 125–33.
34. S.M. Howard: Ellingham Diagrams, Internet resource for MET 320—Metallurgical Thermodynamics, South Dakota School of Mines and Technology, Rapid City, SD. [http://showard.sdsmt.edu/MET320/Handouts/EllinghamDiagrams/Ellingham\\_v22\\_Macro.pdf](http://showard.sdsmt.edu/MET320/Handouts/EllinghamDiagrams/Ellingham_v22_Macro.pdf). Accessed 13 Feb 2014.
35. Physical Constants of Inorganic Compounds. [https://www.slac.stanford.edu/BFROOT/www/Detector/Backgrounds/BkG4Sim/Planning/Validations/neutronCounters/04\\_02\\_85.pdf](https://www.slac.stanford.edu/BFROOT/www/Detector/Backgrounds/BkG4Sim/Planning/Validations/neutronCounters/04_02_85.pdf). Accessed 17 Aug 2015.
36. D.E.C. Corbridge: *Phosphorus 2000: Chemistry, Biochemistry and Technology*, Elsevier, Amsterdam, 2000.
37. C. Stinner: Binary and Ternary Transition-Metal Phosphides as Hydrodenitrogenation Catalysts, PhD Thesis, Swiss Federal Institute of Technology Zurich, Switzerland, 2001, p. 5. <http://e-collection.library.ethz.ch/view/eth:25633>. Accessed 27 Aug 2015.
38. wG. Pantazopoulos, A. Toulfatzis, S. Zornalia, A. Vazdirvanidis, and D. Skarmoutsos: *J. Mater. Eng. Perform.*, 2012, vol. 21 (10), pp. 2188–94.
39. P. Villars: Material Phases Data System (MPDS), CH-6354 Vitznau, Switzerland; SpringerMaterials; sd\_1703036, sd\_0304865 (Springer, Heidelberg, 2014). [http://materials.springer.com/isp/crystallographic/docs/sd\\_1703036](http://materials.springer.com/isp/crystallographic/docs/sd_1703036); [http://materials.springer.com/isp/crystallographic/docs/sd\\_0304865](http://materials.springer.com/isp/crystallographic/docs/sd_0304865). Accessed 18 Aug 2015.
40. R. Monzen, T. Tada, T. Seo, and K. Higashimine: *Mater. Lett.*, 2004, vol. 58 (14), pp. 2007–11.
41. Z.M. Rdzawski, J. Stobrawa, and W. Głuchowski: *J. Achiev. Mater. Manuf. Eng.*, 2009, vol. 33 (1), pp. 7–18.
42. J.S. Romero, M.A. Cruchaga, and D.J. Celentano: *Metall. Mater. Trans. B*, 2013, vol. 44B, pp. 624–52.
43. A.S. Pashinkin and V.A. Fedorov: Phase Equilibria in the Cu-Te System, *Inorganic Materials*, 2003, vol. 39, no. 6, pp. 539–54. Translated from *Neorganicheskie Materialy*, 2003, vol. 39, no. 6, pp. 647–63. Original Text Copyright © 2003 by Pashinkin, Fedorov.